Editorial

Emerging Amikacin Resistance in IMP-Type Carbapenem-Resistant Enterobacterales: A New Concern in Japan

*Tohru Fujiwara, MD, PhD**

* Department of Laboratory Medicine and Infectious Diseases, Iwate Medical University School of Medicine, Yahaba 028-3695, Japan. E-mail: fujiwara@iwate-med.ac.jp

〔Lab Med Int 2026; 5(2): 47-48〕

See article volume 5(2): 49-57

The global spread of carbapenem-resistant Enterobacterales (CRE) remains one of the most pressing challenges in contemporary infectious diseases and clinical microbiology. While the molecular epidemiology of CRE differs substantially across geographic regions, Japan has long exhibited a characteristic resistance profile dominated by IMP-type metallo-β-lactamase (MBL)-producing Enterobacterales, particularly those harboring $bla_{\text{IMP-6}}$ on pKPI-6–related plasmids. Unlike many carbapenemase-producing strains reported in Europe, the United States, and other parts of Asia, these Japanese IMP-type CRE isolates frequently retain susceptibility to amikacin (AMK), despite carrying aminoglycoside resistance-associated genes such as *aac(6′)-Ib*.

In this issue of Laboratory Medicine International, Yokoyama et al. provide important insights into this unique microbiological phenomenon through a detailed molecular analysis of carbapenem-resistant *Escherichia coli* isolates collected during a 13-year surveillance period in Osaka, Japan. Their study highlights the emergence of two multidrug-resistant *E. coli* strains that acquired clinically relevant resistance to AMK in addition to carbapenem and fluoroquinolone resistance. Importantly, the authors demonstrate that resistance was associated not simply with the presence of the commonly detected *aac(6′)-Ib* (L119S) variant, but rather with acquisition of additional aminoglycoside acetyltransferase genes, including *aac(6′)-Iae* and *aac(6′)-Ib-cr*.

This observation is clinically meaningful for several reasons. First, AMK has often remained one of the limited therapeutic options against IMP-type CRE infections in Japan. The relative preservation of AMK susceptibility among IMP-6-producing Enterobacterales has influenced empirical treatment strategies and infection control perspectives in Japanese clinical settings. The present study suggests that this situation may change over time. The acquisition of supplementary resistance determinants capable of conferring higher AMK minimum inhibitory concentrations (MICs) could gradually reduce one of the few remaining antimicrobial vulnerabilities of these organisms.

Second, the study illustrates how subtle genetic differences may significantly alter antimicrobial susceptibility profiles. The *aac(6′)-Ib* (L119S) variant itself appeared to confer only modest increases in AMK MICs, remaining below clinical resistance breakpoints. In contrast, acquisition of *aac(6′)-Iae* or *aac(6′)-Ib-cr* was associated with substantially elevated AMK resistance. These findings emphasize that the mere presence of aminoglycoside resistance genes may not fully predict phenotypic resistance and that detailed molecular characterization remains essential for understanding resistance evolution.

The identification of *aac(6′)-Iae* in *E. coli* is also noteworthy. This gene has been reported predominantly in *Pseudomonas aeruginosa* and appears to be relatively uncommon in Enterobacterales. Its detection on an IncC plasmid raises concern regarding horizontal transfer of resistance determinants across bacterial species. Such interspecies dissemination represents a critical mechanism driving the diversification of antimicrobial resistance in healthcare environments.

Another important aspect of this report is the continued predominance of ST131 among carbapenem-resistant E. coli isolates. ST131 is already recognized globally as a highly successful multidrug-resistant lineage associated with fluoroquinolone resistance and extended-spectrum β-lactamase production. The coexistence of ST131 with IMP-type carbapenemases and additional aminoglycoside resistance determinants may further enhance its clinical impact. Moreover, the detection of ST648 carrying distinct resistance determinants suggests that international dissemination and diversification of resistant lineages are ongoing processes that may increasingly influence the Japanese epidemiological landscape.

From a laboratory medicine perspective, this study also underscores the importance of integrating phenotypic susceptibility testing with genomic surveillance. Carbapenemase-producing organisms do not necessarily exhibit uniform resistance profiles, and small genetic variations may substantially alter therapeutic options. Continuous molecular monitoring is therefore essential not only for epidemiological surveillance but also for guiding antimicrobial stewardship and informing infection control measures.

Several limitations should be acknowledged. The study was conducted at a single institution, and only two AMK-resistant isolates were identified. Nevertheless, the detailed genomic and functional analyses provide valuable mechanistic insights and generate important hypotheses regarding the future evolution of IMP-type CRE in Japan.

In summary, the work by Yokoyama et al. highlights a potentially important shift in the resistance characteristics of IMP-type carbapenem-resistant E. coli. Although AMK susceptibility remains relatively preserved in many Japanese IMP-producing CRE isolates, acquisition of additional aminoglycoside resistance determinants may compromise this advantage. Their findings serve as a timely reminder that antimicrobial resistance is continuously evolving and that resistance phenotypes previously considered characteristic of regional strains may change through ongoing genetic diversification. Continued genomic surveillance and careful interpretation of susceptibility profiles will therefore remain indispensable in the management of CRE infections.

References

1) Yamagishi T, Matsui M, Sekizuka T, et al. A prolonged multispecies outbreak of IMP-6 carbapenemase-producing Enterobacterales due to horizontal transmission of the IncN plasmid. Sci Rep. 2020; 10(1): 4139.

Original

Analysis of amikacin resistance determinants in carbapenem-resistant *Escherichia coli* detected in Japan

Hinako Yokoyama[*1], *Azuki Morishita*[*2], *Shoichi Sakaguchi*[*3],
Takashi Nakano[*3], *Hiroyuki Itagaki*[*4], †*Yuji Nakada*[*1,2]

†Correspondence: Department of Nursing, Faculty of Health Sciences, Aino University, 4-5-4, Higashioda, Ibaraki-shi, Osaka 567-0012, Japan
Tel: +81-72-627-1711; Fax: +81-72-627-1753
E-mail: y-nakada@ns-u.aino.ac.jp (Y.N.)
Received November 29, 2025; accepted February 24, 2026
*1 Department of Nursing, Faculty of Health Sciences, Aino University, Osaka, Japan
*2 Graduate School of Nursing, Department of Nursing, Aino University, Osaka, Japan
*3 Department of Microbiology and Infection Control, Faculty of Medicine, Osaka Medical and Pharmaceutical University, Osaka, Japan
*4 Department of Clinical Laboratory, Division of Central Medical Care, Aino Hospital, Osaka, Japan

ABSTRACT

The global spread of antimicrobial-resistant pathogens remains a major challenge in clinical practice. Among these, carbapenem-resistant Enterobacterales (CRE) are of particular concern, with their prevalence increasing markedly across Asia. In Japan, most CRE isolates produce imipenemase (IMP)-type metallo-β-lactamases (MBLs). Moreover, many strains detected in western Japan carry pKPI-6–related plasmids and their derivatives harboring $bla_{\text{IMP-6}}$, which confer resistance to carbapenems but characteristically retain susceptibility to the aminoglycoside amikacin. We conducted a 13-year surveillance study (2012–2024) of *Escherichia coli* isolates at a mixed-care medical facility in northern Osaka Prefecture, primarily serving patients requiring chronic care. Among 59 carbapenem-resistant *E. coli* strains identified, two exhibited resistance to both carbapenems and amikacin. Both isolates carried $bla_{\text{IMP-6}}$ and the aminoglycoside 6′-N-acetyltransferase (*aac(6′)-Ib*) genes with an *aac(6′)-Ib* variant associated with reduced amikacin resistance, arranged in tandem on the same plasmid. Furthermore, one strain harbored the *aac(6′)-Iae*, which appears to represent a rarely documented occurrence in *E. coli,* whereas the other carried *aac(6′)-Ib-cr.* Cloning experiments and minimum inhibitory concentrations (MICs) analyses identified *aac(6′)-Ia*e and *aac(6′)-Ib-cr* as the likely principal contributors to amikacin resistance in these isolates, whereas the contribution of the *aac(6′)-Ib*(L119S) variant appeared limited. Genome database analysis of IMP-type MBL-producing CRE prevalent in Japan suggested parallel dissemination of bla_{IMP} and the *aac(6′)-Ib*(L119S) variant, which may partly explain the high proportion of isolates that remain susceptible to amikacin. Continued surveillance is warranted to monitor potential shifts in resistance profiles, including the emergence of isolates with increased resistance to amikacin.

〔Lab Med Int 2026; 5(2): 49-57〕

Key Words
aac(6′)-Iae, *aac(6′)-Ib*, *aac(6′)-Ib-cr*, bla_{IMP}, CRE

I. Introduction

The increasing prevalence of antimicrobial-resistant bacteria represents a major global health challenge. In 2024, the World Health Organization (WHO) updated the "Bacterial Priority Pathogens List", highlighting carbapenem-resistant *Acinetobacter*, carbapenem-resistant and third-generation cephalosporin-resistant Enterobacterales, and rifampicin-resistant *Mycobacterium tuberculosis* as pathogens of particular concern [1]. Among these, car-

bapenem-resistant Enterobacterales (CRE) have shown a particularly marked increase in prevalence, especially in Asia[2].

Enterobacterales, including *Escherichia coli* and *Klebsiella* species, are major causes of clinical infections, such as urinary tract infections and sepsis. A subset of these organisms exhibits resistance to imipenem (IPM) and meropenem (MEPM) by producing carbapenemases. Globally, CRE strains producing carbapenemases such as New Delhi metallo-β-lactamase (NDM), *Klebsiella pneumoniae* carbapenemase (KPC), and oxacillinase (OXA) are frequently multidrug-resistant[3)4)]. These strains often display resistance to fluoroquinolones, including ciprofloxacin (CPFX) and levofloxacin (LVFX), due to chromosomal mutations in the quinolone resistance-determining region (QRDR), as well as resistance to aminoglycosides, such as amikacin (AMK), mediated by aminoglycoside acetyltransferases or 16S rRNA methyltransferases[3)5)-7)]. In contrast, in Japan, most CRE isolates harbor imipenemase (IMP)–type metallo- β -lactamases (MBLs) encoded on transmissible plasmids[8)]. In western Japan in particular, pKPI-6–related plasmids and their derivatives carrying $bla_{\text{IMP-6}}$, *aac(6′)-Ib*, and $bla_{\text{CTX-M-2}}$ have become predominant[9)10)]. Although these strains are typically resistant to fluoroquinolones, the vast majority remain clinically susceptible to the AMK[11)–13)].

Previously, we analyzed carbapenem-resistant *E. coli* isolates collected between 2012 and 2016 at a healthcare facility in northern Osaka Prefecture, Japan, and reported their molecular epidemiology and some resistance determinants[12)]. Continued surveillance through 2024 led to the identification of two extensively drug-resistant *E. coli* strains that exhibited resistance to carbapenems, fluoroquinolones, and AMK. The present study aims to elucidate the resistance mechanisms underlying this atypical phenotype and to explore potential factors contributing to the preserved amikacin susceptibility observed in most IMP-type MBL–producing CRE strains detected in Japan.

II. Subjects and Methods

Target strains

This study focused on clinical strains of *E. coli* isolated between 2012 to 2024 at a mixed-care medical facility in the northern part of Osaka Prefecture, Japan. This facility has approximately 900 beds and mostly serves patients requiring chronic care. The AUH-81 strain was the first carbapenem-resistant *E. coli* detected at this institution[12)]. It was therefore selected as a representative AMK-susceptible strain, because it reflects the susceptibility profile commonly observed among IMP-type CRE isolates in Japan. AUH-256 and AUH-310 were identified as extensively drug-resistant strains exhibiting resistance to MEPM, AMK, and LVFX. *Escherichia coli* DH5α was used as the reference laboratory strain (**Table 1**).

Antimicrobial susceptibility testing

Antimicrobial susceptibility testing for the target strains was performed using the MicroScan WalkAway plus System (Beckman Coulter). The drug panel used was Neg EN Combo 1J, which included MEPM, AMK, and LVFX. Testing was conducted in accordance with the Clinical and Laboratory Standards Institute (CLSI) guidelines[14)], and the results were interpreted as susceptible (S), intermediate (I), or resistant (R). Minimum inhibitory concentrations (MICs) for AMK and CPFX were determined using the broth microdilution according to the CLSI guidelines to further characterize resistance levels.

Whole-genome DNA sequencing and multilocus sequence typing (MLST) analysis

The target strains AUH-81, AUH-256, and AUH-310 were cultured in LB medium supplemented with 4 μg/mL of MEPM, and genomic DNA was extracted using the QIAamp DNA Mini Kit (QIAGEN). Long-read sequencing was performed using the MinION (Oxford Nanopore Technologies) with an R9.4.1 flow cell and the Ligation Sequencing Kit (SQK-LSK110), whereas short-read sequencing was conducted using the NovaSeq 6000 (Illumina). Hybrid assembly was carried out with Unicycler[15)], which integrates both long- and short-read data, to obtain complete genome sequences, including plasmids. Gene annotation was performed using DFAST[16)]. The sequences of the MLST target regions of these strains were extracted from the whole-genome sequencing data, and sequence types (STs) were determined using EnteroBase[17)].

Analysis of aminoglycoside acetyltransferase-harboring plasmids

Based on whole-genome DNA sequencing results, all isolates were screened for aminoglycoside acetyltransferase genes known to confer AMK resistance. For isolates carrying these genes, the corresponding plasmids were further characterized and compared with pKPI-6 (AB616660), the predominant plasmid reported in western Japan. Plasmid replicon types were identified using PlasmidFinder 2.0[18)]. Plasmid copy number was estimated by calculating average read depth using SAMtools[19)], and determining the ratio of mean plasmid coverage to

mean chromosomal coverage. Promoter variants were classified according to previously reported Pc promoter sequences [20], and the promoter regions were compared among the isolates (**Table 2**).

Cloning of genes conferring resistance to AMK

The *aac(6′)-Ib* gene from AUH-81 was cloned by digesting genomic DNA using EcoRI and SalI and inserting a 3,453-bp DNA fragment into the corresponding sites of pUC118. This insert was subsequently transferred to the EcoRI and XhoI sites of the low-copy plasmid pNIT6011 (accession no. AB043475) [21][22] to construct pINN464. Similarly, a 1,677-bp SphI/EcoRI fragment containing the *aac(6′)-Iae* from AUH-256 was inserted into the SphI/EcoRI sites of pNIT6011 to generate pINN466. Moreover, a 1,314-bp SphI/HindIII fragment containing the *aac(6′)-Ib* from AUH-256 was cloned into the SphI/HindIII sites of pNIT6011 to construct pINN468. Furthermore, a 2,382-bp SphI/BglII fragment containing the *aac(6′)-Ib-cr* from AUH-310 was inserted into the SphI/BglII sites of pNIT6011 to obtain pINN472. In addition, the *aac(6′)-Ib* gene from AUH-310 was amplified by PCR using KOD-plus DNA polymerase (TAKARA) with primers sul1_R [23] and aac6Ib_R [24], yielding a 1,020-bp product that was cloned into the SphI/EcoRI sites of pNIT6011 to construct pINN474. All constructs were introduced into *E. coli* DH5α for MIC determination. Cloning procedures were performed as described previously [25], ensuring that each insert included the existing Pc promoter upstream of the target gene (**Table 1**, **Figure 1**).

Data availability

The whole-genome DNA sequencing data are deposited in DDBJ accession numbers as follows: *E. coli* AUH-81, genome (accession no. AP044703) and plasmids pAU81-1 (AP044704), pAU81-2 (AP044705), pAU81-

Table 1 *E. coli* strains and plasmids used in this study

Strains & plasmids	Relevant characteristics	Reference or sources
Strains		
DH5α	*F-/endA1 hsdR17 (rk-, mk+) supE44 thi-1 recA1 gyrA relA1D(lacIZYA-argF)U169 deoR (F80dlacD(lacZ)M15)*	Bethesda Research Laboratories
AUH-81	$MEPM^R$, $LVFX^R$	Maki et al. 2020
AUH-256	$MEPM^R$, AMK^R, $LVFX^R$	Maki et al. 2020
AUH-310	$MEPM^R$, AMK^R, $LVFX^R$	This study
Plasmids		
pUC118	Ap^R, ColE1 replicon	Vieira et al. 1987
pNIT6011	Tc^R, pACYC177 and pVS1 replicons	Itoh et al. 2001 (AB043475)
pKPI-6	$MEPM^R$, IncN replicon	Kayama et al. 2015 (AB616660)
pINN464	Tc^R, pNIT6011 derivative carrying *aac(6′)-Ib* of AUH-81	This study
pINN466	Tc^R, pNIT6011 derivative carrying *aac(6′)-Iae* of AUH-256	This study
pINN468	Tc^R, pNIT6011 derivative carrying *aac(6′)-Ib* of AUH-256	This study
pINN472	Tc^R, pNIT6011 derivative carrying *aac(6′)-Ib-cr* of AUH-310	This study
pINN474	Tc^R, pNIT6011 derivative carrying *aac(6′)-Ib* of AUH-310	This study

$MEPM^R$, meropenem; AMK^R, amikacin; $LVFX^R$, levofloxacin; Ap^R, ampicillin; Tc^R, tetracycline.

Table 2 Analysis of plasmids and acetyltransferase promoters and amikacin MICs in carbapenem-resistant *E. coli* isolates

Strains	Plasmids	Replicon types	Plasmid copy numbers	Target genes	Promoter variants	-35 sequence	Spacer region	-10 sequence	Amikacin MICs (μg/mL)
AUH-81	pAU81-1	IncFIA/IncFIB/IncFII/IncN †	1.81	*aac(6′)-Ib* ††	PcH1	TGGACA	17	TAAACT	4
AUH-256	pAU256-1	IncC	5.91	*aac(6′)-Iae*	PcH1	TGGACA	17	TAAACT	128
	pAU256-3	IncN	1.01	*aac(6′)-Ib* ††	PcH1	TGGACA	17	TAAACT	
AUH-310	pAU310-1	IncFIA/IncFIB/IncFII/IncN †	2.00	*aac(6′)-Ib* ††	PcH1	TGGACA	17	TAAACT	64
				aac(6′)-Ib-cr	P_A †††	TTGCAA	17	CATAAT	

MICs, minimum inhibitory concentrations

† Circular multireplicon plasmid (IncFIA/IncFIB/IncFII/IncN replicons).

†† *aac(6′)-Ib* identified in this study was the L119S variant.

††† The sequence TTGCAA–N_{17}–CATAAT was designated as P_A in this study.

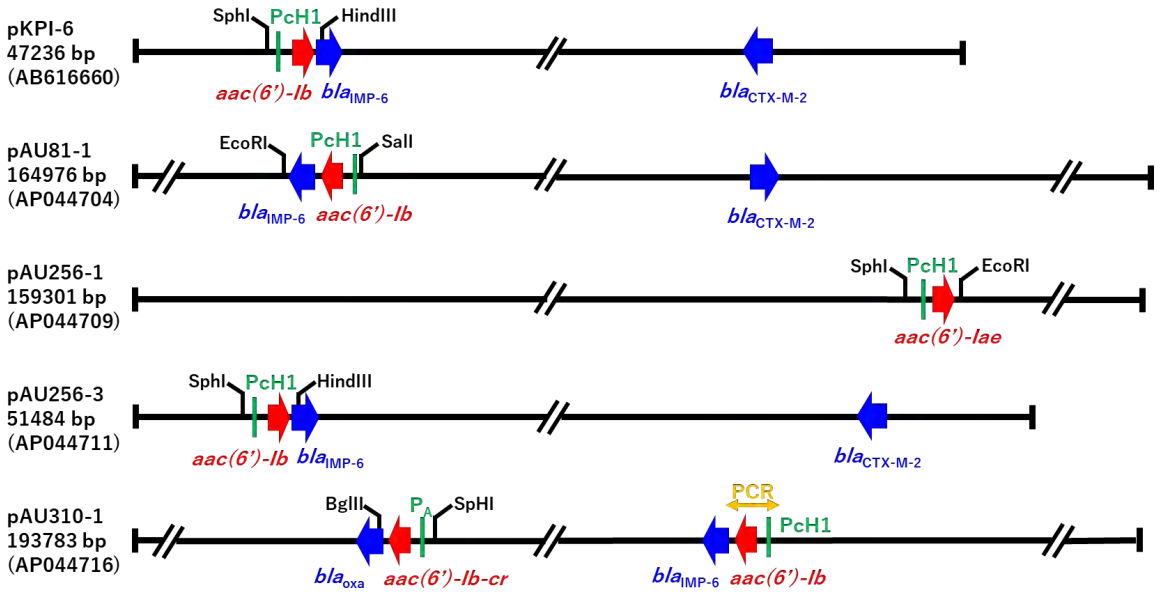

Figure 1 Comparison of plasmids harboring antimicrobial resistance genes and their cloning sites.
Plasmids were obtained from *E. coli* strains AUH-81 (pAU81-1), AUH-256 (pAU256-1 and pAU256-3), and AUH-310 (pAU310-1). In addition, pKPI-6 is shown as a representative plasmid predominantly detected in CRE isolates in western Japan.
β -lactamase genes are indicated by blue arrows, aminoglycoside acetyltransferase genes by red arrows, PCR-amplified regions by yellow double-headed arrows, promoter regions by green lines, and restriction enzyme sites by black bent lines. *aac(6´)-Ib* identified in this study corresponds to the L119S variant. DNA fragments were inserted into pNIT6011 as appropriate.

Table 3 Comparison of carbapenem-resistant *E. coli* isolates AUH-81, AUH-256, and AUH-310

Strains	MLSTs	Breakpoints			MBLs	AACs	mutations		
		MEPM	AMK	LVFX			*aac(6')-Ib*	*gyrA*	*parC*
AUH-81	ST131	R	S	R	bla_{IMP-6}	*aac(6´)-Ib*	L119S	S83L D87N	S80I
AUH-256	ST131	R	R	R	bla_{IMP-6}	*aac(6´)-Ib* *aac(6´)-Iae*	L119S	S83L D87N	S80I
AUH-310	ST648	R	R	R	bla_{IMP-6}	*aac(6´)-Ib* *aac(6´)-Ib-cr*	L119S	S83L D87N	S80I

MLST, multilocus sequence typing; MBL, metallo-β-Lactamase; AAC, aminoglycoside acetyltransferase; MEPM, meropenem; AMK, amikacin; LVFX, levofloxacin.

3 (AP044706), pAU81-4 (AP044707); *E. coli* AUH-256, genome (AP044708) and plasmids pAU256-1 (AP044709), pAU256-2 (AP044710), pAU256-3 (AP044711), pAU256-4 (AP044712), pAU256-5 (AP044713), pAU256-6 (AP044714); *E. coli* AUH-310, genome (AP044715) and plasmids pAU310-1 (AP044716), pAU310-2 (AP044717), pAU310-3 (AP044718), pAU310-4 (AP044719), pAU310-5 (AP044720), pAU310-6 (AP044721).

Statistical analysis

All data were analyzed using descriptive statistics. No further statistical hypothesis testing was performed.

III. Results

Antimicrobial susceptibility testing

Antimicrobial susceptibility testing was conducted on a total of 5,675 *E. coli* isolates collected over a 13-year period (2012–2024), mostly from patients receiving long-term chronic care. Fifty-nine carbapenem-resistant *E. coli* strains were identified. Among these, two extensively drug-resistant strains (AUH-256 and AUH-310) were detected and exhibited resistance to all tested carbapenems (MEPM), fluoroquinolones (LVFX), and aminoglycosides (AMK) (**Table 3**).

Whole-genome DNA sequencing and MLST analysis

Hybrid assembly confirmed that AUH-81 harbored a 5,186,478-bp chromosome and four circular plasmids. Among these, a 164,976-bp circular multireplicon plasmid (IncFIA/IncFIB/IncFII/IncN) designated pAU81-1, carried bla_{IMP-6}, *aac(6′)-Ib*, and $bla_{CTX-M-2}$. AUH-256 harbored a 5,034,660-bp chromosome and six plasmids, including a 159,301-bp IncC plasmid pAU256-1 and a 51,484-bp IncN plasmid pAU256-3. Comparative analysis demonstrated that pKPI-6 and pAU256-3 shared 99.9% average nucleotide identity (ANI) across 98.8% of their aligned regions, indicating that pAU256-3 is a pKPI-6–related plasmid. Moreover, the 1,314-bp SphI/HindIII fragment harboring *aac(6′)-Ib* was identical in sequence between the two plasmids. AUH-310 contained a 5,098,348-bp chromosome and six plasmids, including a 193,783-bp circular multireplicon plasmid (IncFIA/IncFIB/IncFII/IncN) designated pAU310-1 (**Figure 1**, **Table 2**).

Multilocus sequence typing (MLST) analysis showed that AUH-81 and AUH-256 belonged to ST131, which is frequently associated with carbapenem-resistant *E. coli* in Japan [26], whereas AUH-310 was classified as ST648 (**Table 3**).

Analysis of carbapenem and fluoroquinolone resistance determinants

Whole-genome sequencing revealed that AUH-81, AUH-256, and AUH-310 each harbored plasmids encoding bla_{IMP-6} (**Figure 1**). In addition, all three strains harbored mutations in the chromosomal *gyrA* and *parC* genes [27,28], which are known to confer high-level fluoroquinolone resistance (**Table 3**). These findings indicate that the presence of plasmid-mediated bla_{IMP-6}, together with chromosomal mutations in *gyrA* and *parC*, represents the major mechanisms underlying resistance to carbapenems and fluoroquinolones in these strains.

Analysis of AMK resistance determinants

Whole-genome sequencing revealed that AUH-81, AUH-256, and AUH-310 each carried the *aac(6′)-Ib* gene on their plasmids (**Figure 1**). These plasmids were low-copy-number and shared the integron-associated PcH1 promoter variant, which is associated with moderate promoter strength (**Table 2**). All three isolates also carried the previously reported *aac(6′)-Ib* (L119S) substitution [29]. This mutation has been shown to reduce susceptibility to AMK, whereas it increases resistance to gentamicin. MIC testing of the cloned strains carrying *aac(6′)-Ib* (L119S) (DH5α/pINN464, DH5α/pINN468, and DH5α/pINN474) demonstrated only a modest increase in AMK MICs. These findings indicate that this gene alone does not confer clinically relevant resistance (MIC ≥ 32 μg/mL) according to the CLSI standards (**Table 4**).

Conversely, AUH-256, which was resistant to AMK, carried both *aac(6′)-Ib* (L119S) and *aac(6′)-Iae*. The cloned strain harboring *aac(6′)-Iae* (DH5α/pINN466) exhibited a marked increase in AMK MIC. Considering the estimated plasmid copy number and the strength of the PcH1 promoter, these findings suggest that *aac(6′)-Iae* is likely the principal determinant of AMK resistance in AUH-256. Similarly, AUH-310 carried both *aac(6′)-Ib* (L119S) and *aac(6′)-Ib-cr*. The cloned strain harboring *aac(6′)-Ib-cr* (DH5α/pINN472) exhibited elevated AMK MICs, suggesting that *aac(6′)-Ib-cr* is the likely primary determinant of AMK resistance in AUH-310. Moreover, *aac(6′)-Ib-cr* is also known to increase resistance to CPFX [30], and in this study, the cloned strain DH5α/pINN472 exhibited a slight increase in CPFX resistance as well (**Table 4**).

Table 4 Minimum inhibitory concentrations of target resistant gene clones

Strains	Target genes			MICs (μg/mL)	
	aac(6')-Ib †	*aac(6')-Ib-cr*	*aac(6')-Iae*	AMK	CPFX
DH5α	−	−	−	0.5	0.025
DH5α/pNIT6011	−	−	−	0.5	0.025
AUH-81	+	−	−	4	64
DH5α/pINN464	+	−	−	4	n.d.
AUH-256	+	−	+	128	128
DH5α/pINN466	−	−	+	64	0.025
DH5α/pINN468	+	−	−	2	n.d.
AUH-310	+	+	−	64	512
DH5α/pINN472	−	+	−	16	0.05
DH5α/pINN474	+	−	−	2	n.d.

MICs, minimum inhibitory concentrations; AMK, amikacin; CPFX, ciprofloxacin; n.d., not done.
† *aac(6')-Ib* identified in this study was the L119S variant.

IV. Discussion

At a medical facility in Osaka City—the site of the first reported healthcare-associated infections caused by CRE in Japan—the causative organisms were *E. coli* and *Klebsiella* spp. harboring pKPI-6–related plasmids and their derivative plasmids carrying the IMP-6–type MBL gene and the CTX-M-2 group extended-spectrum beta-lactamase (ESBL) gene [10]. Subsequent reports have shown that CRE isolates detected in western Japan share similar characteristics [8], a pattern also observed in the present study. These IMP-6–type MBLs belong to the IMP-1 group, in which part of the amino acid sequence of IMP-1 is substituted, and are known to hydrolyze MEPM more efficiently than IPM [31]. Consequently, strains producing IMP-6–type MBL may appear susceptible to IPM, potentially leading to delayed detection and implementation of infection control measures. Careful interpretation of susceptibility profiles is therefore essential.

Many of the CRE strains detected in Japan remain susceptible to AMK despite harboring *aac(6′)-Ib*. Analysis of genome database entries of CRE isolates detected and registered in Japan identified several strains, including IMP-6–type MBL-producing *E. coli* (accession no. AP022350) [32], IMP-6–type MBL-producing *K. pneumoniae* (accession no. AP022358) [32], and IMP-1–type MBL-producing *E. coli* (accession no. LC720959) [33], which carry the *aac(6′)-Ib* (L119S) variant, which carries a mutation located immediately upstream of the IMP-type MBL gene. This variant is considered one of the factors contributing to the continued susceptibility of many IMP-type MBL–producing CRE isolates to AMK in Japan. Consistent with these findings, a previous study reported that AMK MIC of a strain harboring *aac(6′)-Ib* (L119S) was approximately one-eighth of that observed in a strain carrying the wild-type gene [29], with the MIC remaining below the CLSI breakpoint. However, despite MIC values below the CLSI breakpoint, the potential for residual enzymatic activity suggests that caution may be warranted in clinical practice, for example, by avoiding AMK monotherapy and considering its use in combination with other antimicrobial agents [34][35].

In the AUH-256 strain, which was resistant to AMK, both *aac(6′)-Ib* (L119S) and *aac(6′)-Iae* were detected, and *aac(6′)-Iae* has previously been reported primarily in *Pseudomonas aeruginosa* isolates in Japan [36]. Its identification in *E. coli* in this study appears to represent a rare occurrence. This gene was located on an IncC plasmid [37], a large multidrug resistance plasmid, suggesting the possibility of interspecies transmission from *P. aeruginosa*. Furthermore, the AUH-310 strain, which also exhibited resistance to AMK, carried both *aac(6′)-Ib* (L119S) and *aac(6′)-Ib-cr*. The *aac(6′)-Ib-cr* is known to confer resistance to both AMK and CPFX, and when combined with *gyrA* and *parC* mutations, it can substantially enhance fluoroquinolone resistance [30]. Collectively, these findings suggest that in CRE carrying IMP-type MBL—frequently detected in Japan—clinically relevant AMK resistance may arise through acquisition of additional determinants, such as *aac(6′)-Iae* or *aac(6′)-Ib-cr*, whereas *aac(6′)-Ib* (L119S) alone appears insufficient to confer clinically relevant AMK resistance in the isolates examined in this study.

The AUH-81 and AUH-256 strains, analyzed in this study, belonged to ST131, which has been reported as the dominant lineage among clinical *E. coli* isolates [8]. In contrast, the AUH-310 strain belonged to ST648, a lineage reported in the European Economic Area to carry NDM-type MBL and OXA-type ESBL [38]. Although ST648 has been detected only rarely in Japan, one case was reported in a patient with a history of hospitalization in India [39]. Moreover, the AUH-310 strain carried OXA-type ESBL genes, representing resistance determinants distinct from those identified in the AUH-81 and AUH-256 strains. With the increase in international travel, the potential exists for regionally prevalent plasmids to disseminate into strains with diverse genetic backgrounds, potentially contributing to the emergence of new multidrug-resistant lineages.

This study has several limitations. The isolates were obtained from a single medical facility in northern Osaka, and therefore, the findings may not be generalizable to the entire Japanese healthcare setting. Furthermore, only two aminoglycoside-resistant isolates were identified, limiting the strength of conclusions regarding the relative contribution of individual *aac(6′)* genes to AMK resistance. Further studies involving a larger number of isolates, as well as experimental assessments of plasmid transmissibility and functional analyses, are warranted. In addition, for the extensively drug-resistant strains identified in this study, assessment of plasmid transferability and exploration of effective therapeutic options remain necessary. Nevertheless, the identification of distinct genetic mechanisms underlying AMK resistance in IMP-type MBL–producing isolates highlights the ongoing diversification of resistance determinants. Continuous surveillance and molecular characterization of these determinants will therefore be important for improving our understanding of emerging resistance patterns and for

informing appropriate antimicrobial treatment strategies.

Authorship Contributions

HY, AM, and YN conceived and designed the study, performed the experiments, and interpreted the data. SS, TN, and HI contributed experimental and analytical resources.

All authors critically reviewed the manuscript and approved the final version for publication.

Acknowledgements

This work was supported in part by Aino University Research Grant (Number 10S-24001).

Disclosure

The authors declare no conflict of interest.

References

1) World Health Organization. WHO bacterial priority pathogens list, 2024: bacterial pathogens of public health importance to guide research, development, and strategies to prevent and control antimicrobial resistance. Geneva: World Health Organization; 2024. Licence: CC BY-NC-SA 3.0 IGO.

2) Miller WR, Arias CA. ESKAPE pathogens: antimicrobial resistance, epidemiology, clinical impact, and therapeutics. Nat Rev Microbiol. 2024; 22(10): 598-616. doi: 10.1038/s41579-024-01054-w.

3) van Duin D, Doi Y. The global epidemiology of carbapenemase-producing Enterobacteriaceae. Virulence. 2017; 8(4): 460-9. doi: 10.1080/21505594.2016.1222343.

4) Sawa T, Kooguchi K, Moriyama K. Molecular diversity of extended-spectrum β-lactamases and carbapenemases, and antimicrobial resistance. J Intensive Care. 2020; 8: 13. doi: 10.1186/s40560-020-0429-6.

5) Jean SS, Harnod D, Hsueh PR. Global threat of carbapenem-resistant Gram-negative bacteria. Front Cell Infect Microbiol. 2022; 12: 823684. doi: 10.3389/fcimb.2022.823684.

6) Koumaki V, Voudanta E, Michelaki A, et al. Changing epidemiology of carbapenemases among carbapenem-resistant Enterobacterales in a Greek tertiary care hospital in Athens, 2020 to 2023. Antibiotics (Basel). 2025; 14(3): 239. doi: 10.3390/antibiotics14030239.

7) Tunyong W, Arsheewa W, Santajit S, et al. Antibiotic resistance genes among carbapenem-resistant Enterobacterales (CRE) isolates of Prapokklao Hospital, Chanthaburi Province, Thailand. Infect Drug Resist. 2021; 14: 3485-94. doi: 10.2147/idr.s328521.

8) Yamagishi T, Matsui M, Sekizuka T, et al. A prolonged multispecies outbreak of IMP-6 carbapenemase-producing Enterobacterales due to horizontal transmission of the IncN plasmid. Sci Rep. 2020; 10: 4139. doi: 10.1038/s41598-020-60659-2.

9) Kayama S, Shigemoto N, Kuwahara R, et al. Complete nucleotide sequence of the IncN plasmid encoding IMP-6 and CTX-M-2 from emerging carbapenem-resistant Enterobacteriaceae in Japan. Antimicrob Agents Chemother. 2015; 59(2): 1356-9. doi: 10.1128/AAC.04759-14.

10) Abe R, Akeda Y, Sugawara Y, et al. Characterization of the plasmidome encoding carbapenemase and mechanisms for dissemination of carbapenem-resistant Enterobacteriaceae. mSystems. 2020; 5(6): e00759-20. doi: 10.1128/mSystems.00759-20.

11) Kanazawa S, Sato T, Kohira N, et al. Susceptibility of imipenem-susceptible but meropenem-resistant bla_{IMP-6}-carrying Enterobacteriaceae to various antibacterials, including the siderophore cephalosporin cefiderocol. Antimicrob Agents Chemother. 2017 ; 61: e00576-17. doi: 10.1128/aac.00576-17.

12) Maki M, Itagaki H, Nakada Y. Characteristics and longitudinal kinetic analysis of carbapenem-resistant *Escherichia coli* detected in a northern Osaka Prefecture medical facility. Jpn J Med Technol. 2020; 69: 10-6. doi: 10.14932/jamt.19-29

13) Oka K, Matsumoto A, Tetsuka N, et al. Japan Infection Prevention and Control Conference for National and Public University Hospitals. Clinical characteristics and treatment outcomes of carbapenem-resistant Enterobacterales infections in Japan. J Glob Antimicrob Resist. 2022; 29: 247-52. doi: 10.1016/j.jgar.2022.04.004.

14) Clinical and Laboratory Standards Institute. Performance standards for antimicrobial susceptibility testing. 32nd ed. CLSI document M100. Wayne, PA: Clinical and Laboratory Standards Institute; 2022.

15) Wick RR, Judd LM, Gorrie CL, et al. Unicycler: resolving bacterial genome assemblies from short and long sequencing reads. PLoS Comput Biol. 2017; 13(6): e1005595. doi: 10.1371/journal.pcbi.1005595

16) Tanizawa Y, Fujisawa T, Kaminuma E, et al. DFAST and DAGA: web-based integrated genome annotation tools and resources. Biosci Microbiota Food Health. 2016; 35(4): 173-84. doi: 10.12938/bmfh.16-003.

17) Zhou Z, Charlesworth J, Achtman M. et al. A multi-level clustering scheme for population assignments based on core genome MLST. Bioinformatics. 2021; 37 (20) : 3645-6. doi: 10.1093/bioinformatics/btab234.

18) Carattoli A, Zankari E, García-Fernández A, et al. In silico detection and typing of plasmids using PlasmidFinder and plasmid multilocus sequence typing. Antimicrob Agents Chemother. 2014; 58 (7): 3895-903. doi:10.1128/AAC.02412-14.

19) Li H, Handsaker B, Wysoker A, et al. The Sequence Alignment/Map format and SAMtools. Bioinformatics. 2009; 25

(16): 2078-9. doi:10.1093/bioinformatics/btp352.

20) Jové T, Da Re S, Denis F, et al. Inverse correlation between promoter strength and excision activity in class 1 integrons. PLoS Genet. 2010; 6 (1): e1000793. doi:10.1371/journal.pgen.1000793.

21) Heeb S, Itoh Y, Nishijyo T, et al. Small, stable shuttle vectors based on the minimal pVS1 replicon for use in Gram-negative, plant-associated bacteria. Mol Plant Microbe Interact. 2000; 13 (2): 232-7. doi: 10.1094/mpmi.2000.13.2.232

22) Nishijyo T, Haas D, Itoh Y. The CbrA–CbrB two-component regulatory system controls the utilization of multiple carbon and nitrogen sources in Pseudomonas aeruginosa. Mol Microbiol. 2001; 40 (4): 917-31. doi: 10.1046/j.1365-2958.2001.02435.x

23) Chauhan R, Sharma PC. Characterization of phenotypically metallo-β-lactamase positive Pseudomonas aeruginosa human isolates from Himachal Pradesh for MBL genes (bla_{VIM-2} and bla_{IMP-1}), integrase gene class 1, 2, 3 (*int1*, *int2* and *int3*), and sulphonamide resistance gene (*sul1*). AI Ameen J Med Sci. 2015 ; 8 (3): 195-201.

24) Tada T, Miyoshi-Akiyama T, Tanaka M, et al. Development of an immunochromatographic assay for rapid detection of AAC (6')-Ib-producing Pseudomonas aeruginosa. J Microbiol Methods. 2012; 91 (1): 114-6. doi: 10.1016/j.mimet.2012.05.009

25) Sambrook J, Russell DW. Molecular cloning: a laboratory manual. 3rd ed. Cold Spring Harbor, NY: Cold Spring Harbor Laboratory Press; p.31-116.

26) Fukuda A, Nakamura H, Umeda K, et al. Seven-year surveillance of the prevalence of antimicrobial-resistant Escherichia coli isolates, with a focus on ST131 clones, among healthy people in Osaka, Japan. Int J Antimicrob Agents. 2021; 57 (3): 106298. doi: 10.1016/j.ijantimicag.2021.106298

27) Hopkins KL, Davies RH, Threlfall EJ. Mechanisms of quinolone resistance in Escherichia coli and Salmonella: recent developments. Int J Antimicrob Agents. 2005; 25 (5): 358-73. doi: 10.1016/j.ijantimicag.2005.02.006

28) Cagnacci S, Gualco L, Debbia E, et al. European emergence of ciprofloxacin-resistant Escherichia coli clonal groups O25:H4-ST131 and O15:K52:H1 causing community-acquired uncomplicated cystitis. J Clin Microbiol. 2008 ; 46 (8): 2605-12. doi: 10.1128/jcm.00640-08

29) Rather PN, Munayyer H, Mann PA, et al. Genetic analysis of bacterial acetyltransferases: identification of amino acids determining the specificities of the aminoglycoside 6'-N-acetyltransferase Ib and IIa proteins. J Bacteriol. 1992 ; 174 (10): 3196-203. doi: 10.1128/jb.174.10.3196-3203.1992

30) Machuca J, Ortiz M, Recacha E, et al. Impact of AAC (6')-Ib-cr in combination with chromosomal-mediated mechanisms on clinical quinolone resistance in Escherichia coli. J Antimicrob Chemother. 2016; 71: 3066-71 (11). doi: 10.1093/jac/dkw258

31) Hirabayashi A, Yahara K, Kajihara T, et al. Geographical distribution of Enterobacterales with a carbapenemase IMP-6 phenotype and its association with antimicrobial use: an analysis using comprehensive national surveillance data on antimicrobial resistance. PLoS ONE. 2020; 15 (12): e0243630. doi: 10.1371/journal.pone.0243630

32) Yano H, Ogawa M, Endo S, et al. High frequency of IMP-6 among clinical isolates of metallo-β-lactamase-producing Escherichia coli in Japan. Antimicrob Agents Chemother. 2012; 56 (8): 4554-5. doi: 10.1128/AAC.06212-11

33) Ikegaya K, Aoki K, Komori K, et al. Analysis of the stepwise acquisition of $bla_{CTX-M-2}$ and subsequent acquisition of either bla_{IMP-1} or bla_{IMP-6} in highly conserved IncN-pST5 plasmids. JAC Antimicrob Resist. 2023; 5 (5): dlad106. doi: 10.1093/jacamr/dlad106

34) Farhan SM, Abd El-Baky RM, Abdalla S, et al. In vitro and in vivo effect of amikacin and imipenem combinations against multidrug-resistant *E. coli*. Trop Med Infect Dis. 2022; 7 (10): 281. doi: 10.3390/tropicalmed7100281

35) Nakakura I, Ogawa Y, Sakakura K, et al. IMP-6 carbapenemase-producing Enterobacteriaceae bacteremia successfully treated with amikacin-meropenem in two patients. Pharmacotherapy. 2017; 37 (10): e96-e102. doi:10.1002/phar.1980

36) Kitao T, Tada T, Tanaka M, et al. Emergence of a novel multidrug-resistant Pseudomonas aeruginosa strain producing IMP-type metallo-β-lactamases and AAC (6')-Iae in Japan. Int J Antimicrob Agents. 2012 ; 39 (6): 518-21. doi: 10.1016/j.ijantimicag.2012.01.010

37) Fricke WF, Welch TJ, McDermott PF, et al. Comparative genomics of the IncA/C multidrug resistance plasmid family. J Bacteriol. 2009; 191 (15): 4750-7. doi: 10.1128/JB.00189-09

38) Linkevicius M, Bonnin RA, Alm E, et al. Rapid cross-border emergence of NDM-5-producing *Escherichia coli* in the European Union/European Economic Area, 2012 to June 2022. Euro Surveill. 2023; 28 (19): 2300209. doi: 10.2807/1560-7917.ES.2023.28.19.2300209

39) Mizuno Y, Yamaguchi T, Matsumoto T. A first case of New Delhi metallo-β-lactamase-7 in an *Escherichia coli* ST648 isolate in Japan. J Infect Chemother. 2014; 20 (2): 814-6. doi: 10.1016/j.jiac.2014.05.001

GRAPHICAL ABSTRACT

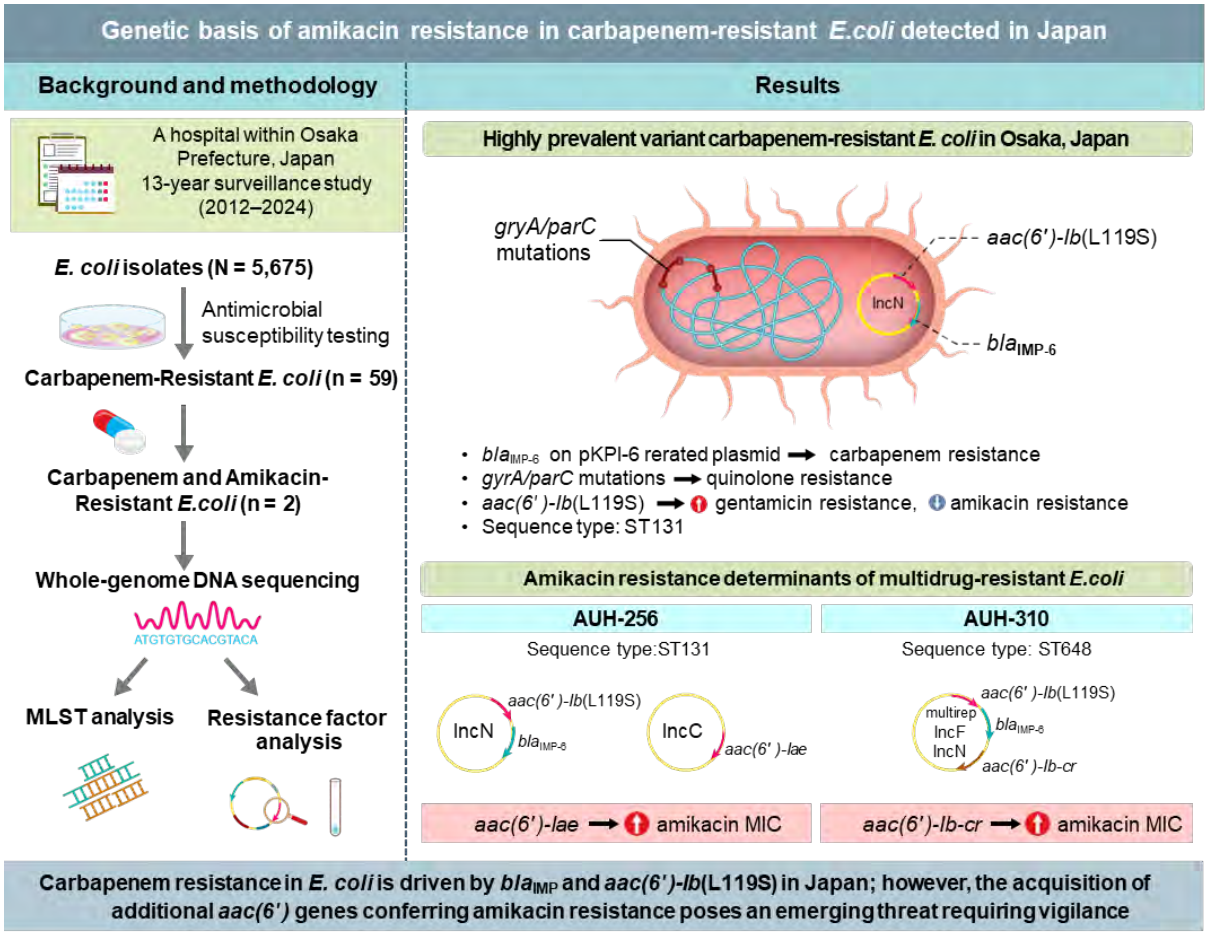

E. coli: *Escherichia coli*; MLST: multi-locus sequence typing; MIC: minimum inhibitory concentration

Laboratory Medicine International, Yokoyama et al.

Original

Diagnostic utility of combined cerebrospinal fluid interleukin-6 and procalcitonin in bacterial meningitis: Sensitivity and specificity analysis

*†Takuya Shimura*1, Hitomi Sakata*2, Masahiro Yamamoto*2, Ryunosuke Ohkawa*3, Akira Yoshimoto*3, Tomonori Suzuki*4, Masato Nishioka*4*

†Correspondence: Department of Clinical Laboratory, Kawaguchi Municipal Medical Center, 180 Nishiaraijuku, Kawaguchi-shi, Saitama 333-0833, Japan
Tel: +81-48-287-2525
E-mail: shimuson_takuya@yahoo.co.jp
Received July 15, 2025; accepted November 10, 2025
*1 Department of Clinical Laboratory, Kawaguchi Municipal Medical Center, Saitama, Japan; Clinical Bioanalysis and Molecular Biology, Graduate School of Medical and Dental Sciences, Institute of Science Tokyo, Tokyo, Japan
*2 Department of Clinical Laboratory, Kawaguchi Municipal Medical Center, Saitama, Japan
*3 Clinical Bioanalysis and Molecular Biology, Graduate School of Medical and Dental Sciences, Institute of Science Tokyo, Tokyo, Japan
*4 Department of Pediatrics, Kawaguchi Municipal Medical Center, Saitama, Japan

ABSTRACT

Background: Bacterial meningitis (BM) is a life-threatening condition requiring early diagnosis and treatment to prevent severe complications; however, traditional diagnostic methods, such as cerebrospinal fluid (CSF) analysis, Gram staining, and bacterial cultures, can be slow/nonspecific. Therefore, novel biomarkers are needed. IL-6 levels increase during inflammatory responses, whereas procalcitonin (PCT) levels specifically increase during bacterial infections. Herein, we investigated the utility of CSF IL-6 and PCT levels to differentiate BM from other central nervous system (CNS) diseases.

Methods: CSF samples were collected from 70 patients (mean age, 37.5 years; SD, 17.8 years; male/female, 36/34) treated at Kawaguchi Municipal Medical Center between September 2022 and 2023. Blood samples were additionally collected from 53 patients. BM was diagnosed based on clinical symptoms, culture results, and antibiotic responses. CSF IL-6 and PCT concentrations were measured using electrochemiluminescence immunoassays.

Results: CSF IL-6 and PCT levels were significantly higher in patients with BM than those with non-bacterial CNS diseases. Receiver operating characteristic analysis revealed that CSF PCT had a higher diagnostic accuracy (area under the curve = 0.887) than CSF IL-6 and cell counts. Concurrent measurement of CSF IL-6 and PCT levels improved the specificity of BM diagnosis from 0.71 to 0.95.

Conclusions: Combining CSF IL-6 and PCT measurements provides better diagnostic accuracy for BM than either marker alone. CSF IL-6 primarily reflects intrathecal production, and although a weak correlation with serum IL-6 was observed, it remains unclear whether serum IL-6 contributes to CSF levels. PCT remains highly specific to bacterial infections.Further large-scale studies are required to validate these findings and confirm the utility of these biomarkers in clinical settings.

〔Lab Med Int 2026; 5(2): 58-66〕

Key Words
Procalcitonin, Interleukin-6, Bacterial meningitis, Central nervous system diseases

I. Introduction

Bacterial meningitis (BM) is a treatable disease if diagnosed and managed early; however, delayed treatment can result in severe sequelae or death. Therefore, early diagnosis and prompt therapeutic intervention are crucial [1]. The diagnostic tests for this disease include biochemical analysis of the cerebrospinal fluid (CSF), Gram staining, bacterial culture, and neuroimaging (computed tomography and magnetic resonance imaging). Among these, the presence of bacteria in the CSF observed on Gram staining or bacterial culture is considered the gold standard method for diagnosis [1), 2)]. However, bacterial culture is time consuming, and is sometimes too slow in clinical settings. An increased CSF cell count is a key indicator for diagnosing BM. However, some rare cases present with no increases in the early stages of BM. Furthermore, cell count elevation is observed in other conditions, such as non-BM or Behçet's disease [3)], making diagnosis challenging. Therefore, the development of novel biomarkers that offer both accurate and rapid results for BM diagnosis is highly desirable in clinical practice.

Interleukin-6 (IL-6) is a glycoprotein with a molecular weight of 21,000–26,000, produced by T cells and macrophages. IL-6, a type of cytokine with diverse physiological functions in the body, increases in autoimmune diseases and infections [4)-6)]. Measuring IL-6 levels in the CSF has been reported as useful for diagnosing inflammatory diseases, such as Behçet's disease, neuromyelitis optica spectrum disorders, and acute brain injuries [7)-9)]. These reports support the notion that IL-6 levels increase in diseases in which lymphocytes and macrophages are activated. In contrast, procalcitonin (PCT), a precursor of calcitonin, is a polypeptide comprising 116 amino acids with a molecular weight of 13,000, and is synthesized in the C cells of the thyroid gland. PCT levels specifically increase during bacterial inflammation [10),11)], and are widely used in clinical settings owing to their rapid measurement. Several prior studies have revealed the usefulness of CSF PCT for diagnosing BM and intracranial infections after craniotomy [12)-15)]. While both IL-6 and PCT have been individually studied as biomarkers for meningitis, there is a lack of studies comparing their diagnostic values within the same cohort. Furthermore, differentiating between BM and non-BM remains a clinical challenge, and reliable biomarkers are required. Therefore, we aimed to measure IL-6 and PCT levels in CSF samples to assess their combined utility in distinguishing BM from other central nervous system (CNS) diseases. Consequently, we sought to elucidate the specific diagnostic advantages of CSF IL-6 and PCT compared with prior studies that have focused on each marker separately.

II. Methods

In the present study, we used CSF samples from 70 patients, with 52 paired blood samples, from patients submitted to the Department of Laboratory Medicine at the Kawaguchi Municipal Medical Center between September 2022 and September 2023. The patients' age and sex were calculated as follows: age: 37.5 years (mean age, SD: 17.8 years), sex: 36 males, 34 females. Inclusion and exclusion criteria were applied according to the study protocol.

The CSF and blood samples used in this study were residual samples after diagnostic testing was completed. CSF samples that exhibited reddish coloration or suspected blood contamination were excluded. Additionally, samples with insufficient volumes that prevented the simultaneous measurement of IL-6 and PCT levels were excluded. The BM group included patients diagnosed with BM based on positive or negative CSF culture results, CSF biochemical tests, imaging findings, clinical symptoms, and improvement after antimicrobial therapy. Other CNS diseases with increased CSF cell counts were diagnosed based on neurological findings, imaging (computed tomography and magnetic resonance imaging) tests, electrophysiological tests, and clinical course. Participants were classified into three groups based on their diagnosis: non-CNS diseases (non-CNS), BM, and non-bacterial CNS diseases (non-BM).

After collecting CSF samples, the CSF cell count, glucose concentration, protein concentration, CSF IL-6 concentration, and CSF PCT concentration were measured. Additionally, IL-6 and PCT concentrations were measured in blood samples collected on the same day. IL-6 and PCT concentrations in both the CSF and blood were measured using the electrochemiluminescence immunoassay method with the Cobas Pro e801 analyzer (Roche Diagnostics Co., Ltd.).

Comparisons between groups were performed using the Steel-Dwass test. Correlations were examined using Spearman's rank correlation coefficients. The normality of the distribution of continuous data was assessed using the Shapiro–Wilk test, with results confirming that the data were not normally distributed. Therefore, the data are presented as medians and interquartile ranges. Statistical analysis was performed using JMP Pro Ver.17, with a two-tailed p-value of <0.05 considered statistically significant. This study was approved by the Ethics Committee

of the Kawaguchi Municipal Medical Center (2021-13).

III. Results

1. Comparison of IL-6 and PCT levels in bacterial and non-bacterial CNS diseases

Concentrations of IL-6 and PCT in the BM group were significantly higher than those in the non-BM group (**Table 1**). The PCT concentration in the non-CNS group was significantly lower in the CSF than in the blood (**Fig. 1**). In non-BM cases, CSF IL-6 levels above the cutoff value were observed in six cases from the non-CNS group and 12 cases from the non-BM group. CSF PCT levels above the cutoff value were observed in four patients from the non-CNS group and five patients from the non-BM group.

2. Diagnostic accuracy of CSF IL-6, PCT, and cell count in BM

Receiver operating characteristic analysis was conducted to evaluate the diagnostic capabilities of CSF IL-6, PCT, and cell counts for the diagnosis of BM. The areas under the curve (AUCs) were calculated for each parameter. The results showed an AUC of 0.881 for CSF IL-6, 0.887 for CSF PCT, and 0.824 for CSF cell count. The CSF PCT level showed the highest diagnostic ability for BM (**Fig. 2**).

3. Correlations between serum and CSF IL-6 and PCT levels

Subsequently, the correlations between the serum and CSF levels of IL-6 and PCT were examined. A weak positive correlation was identified between CSF and serum IL-6 levels, suggesting that serum concentration affects CSF IL-6 levels. No significant correlations were observed between the CSF and serum PCT levels (**Fig. 3**).

4. Combined use of CSF IL-6 and PCT for improved diagnosis of BM

Based on these findings, CSF IL-6 and PCT levels showed a higher diagnostic accuracy for BM than CSF cell count. Consequently, we investigated whether the simultaneous measurement of CSF IL-6 and PCT levels could improve the diagnostic capability for BM compared with each marker measured individually. When the cutoff values for BM were set at 15.4 pg/mL for CSF IL-6 and 0.173 ng/mL for CSF PCT, the specificity for diagnosing BM increased from 0.71 (when measuring only CSF IL-6 concentration) to 0.95 (when both CSF IL-6 and PCT exceeded their respective cutoff values). However, the sensitivity for diagnosing BM when both biomarker exceeded the cutoff value decreased from 1.00 to 0.88 (**Fig. 4** and **Table 2**). The corresponding cutoff values for serum IL-6 and PCT are presented in Supplementary **Figure 1**. The AUC values for serum IL-6 and PCT were 0.6702 and 0.644, respectively. These results indicate that serum IL-6 and PCT alone do not provide sufficient diagnostic performance to reliably distinguish BM from non-BM cases (Supplementary **Fig. 1**).

IV. Discussion

In the present study, we evaluated the diagnostic capability of CSF IL-6 and PCT concentrations as quantitative biomarkers of BM. We confirmed that the CSF concentrations of these biomarkers were significantly higher in patients with BM than in those without BM. Additionally, the combination of CSF IL-6 and PCT measurements showed potential as biomarkers with high sensitivity and specificity, particularly in patients with BM.

Regarding CSF IL-6, previous studies have shown its utility for the diagnosis of BM [16),17)]. Consistent with these reports, our findings confirmed the usefulness of CSF IL-6 in the diagnosis of BM (**Fig. 1(a)**). Based on our results, CSF IL-6 appears to have a relatively high sensitivity for diagnosing BM. CSF IL-6 primarily reflects intrathecal production, and although a weak correlation with serum IL-6 was observed, it remains unclear whether serum IL-6 contributes to CSF levels. (**Fig. 3(a)**). Furthermore, even in the non-BM group, the CSF IL-6 levels tended to increase (**Fig. 1(a)**). This

Table 1 Patient characteristics

	Non-CNS (N=36)	BM (N=8)	Non-BM (N=26)
Age	29.3 ± 33.6	40.8 ± 38.6	44.1 ± 30.6
Male/Female	17/19	5/3	14/12
CSF IL-6 (pg/mL)	12.6 ± 21.4	1146.5 ± 2388.1	572.5 ± 2541.5
IL-6 (pg/mL)	66.9 ± 140.5 (n=25)	58.84 ± 55.0 (n=5)	44.6 ± 59.2 (n=22)
CSF PCT (ng/mL)	0.131 ± 0.070	1.031 ± 2.006	0.132 ± 0.069
PCT (ng/mL)	0.356 ± 0.914 (n=25)	1.451 ± 2.902 (n=5)	0.776 ± 3.111 (n=22)
CSF cells (cell/μL)	1.4 ± 0.9	45.6 ± 89.8	30.7 ± 70.0

CSF, cerebrospinal fluid; IL-6, interleukin-6; PCT, procalcitonin; BM, bacterial meningitis; non-CNS, non-central nervous system diseases; non-BM, non-bacterial central nervous system diseases

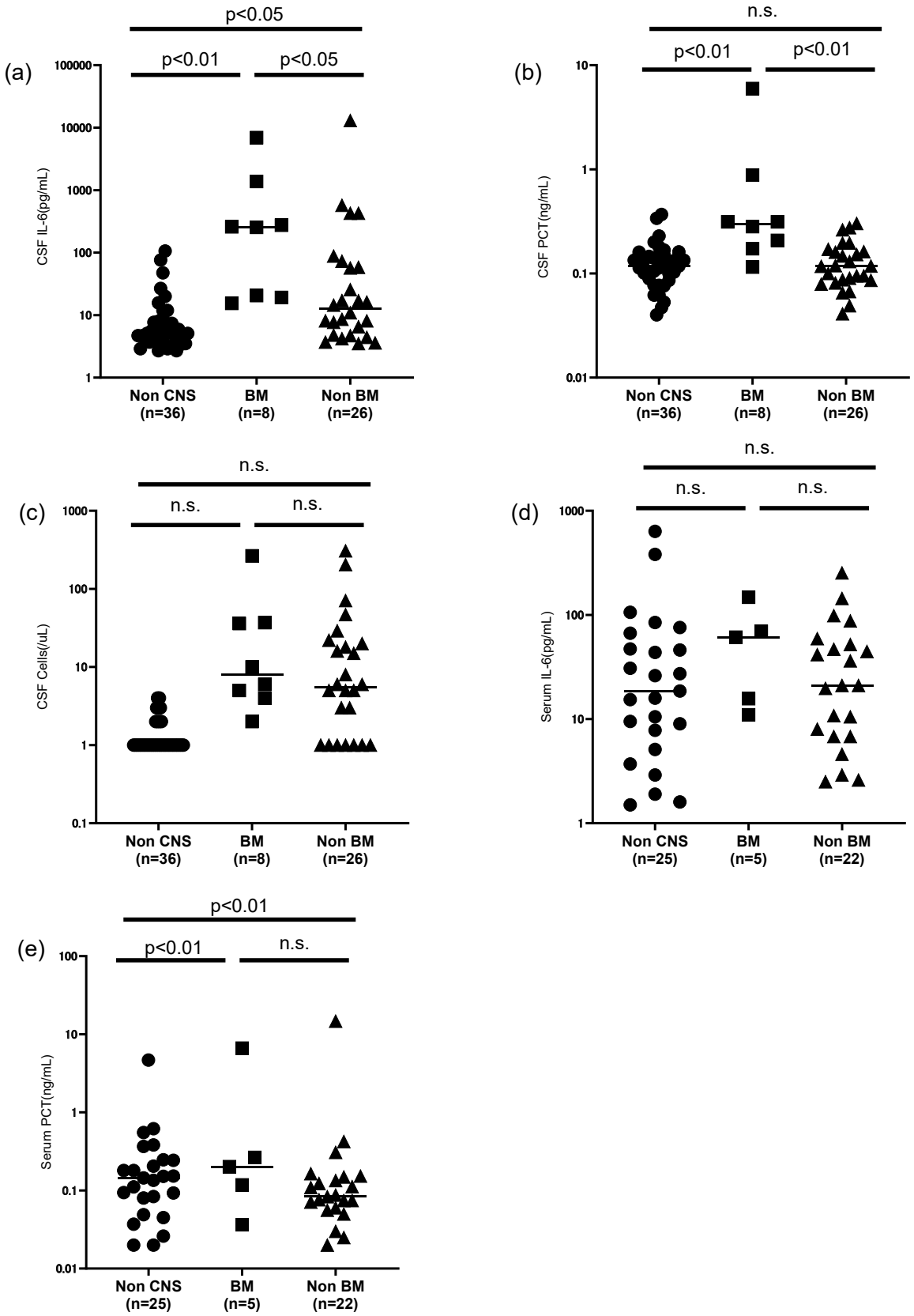

Figure 1 Comparison of IL-6 and PCT concentrations among the non-CNS, BM, and non-BM groups. CSF, cerebrospinal fluid; IL-6, interleukin-6; PCT, procalcitonin; BM, bacterial meningitis; non-CNS, non-central nervous system diseases; non-BM, non-bacterial central nervous system diseases.

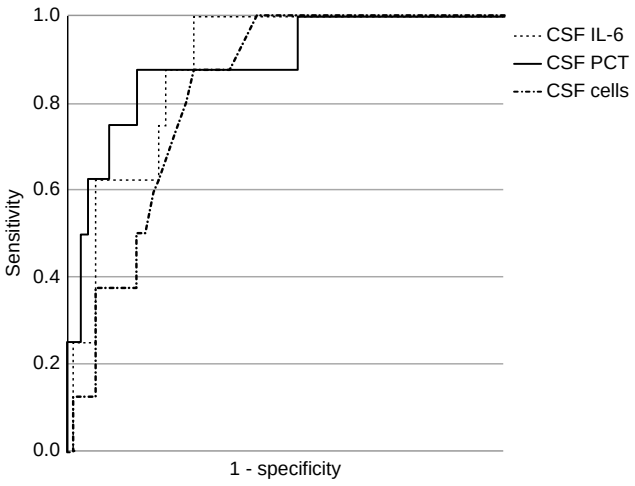

Figure 2 ROC analyses examining the ability of CSF IL-6 and PCT levels to diagnose BM.
ROC analyses were conducted to investigate the use of IL-6 and PCT levels in the CSF to discriminate between the BM and non-BM groups.
CSF, cerebrospinal fluid; IL-6, interleukin-6; PCT, procalcitonin; BM, bacterial meningitis; ROC, receiver operating characteristic; non-BM, non-bacterial central nervous system diseases.

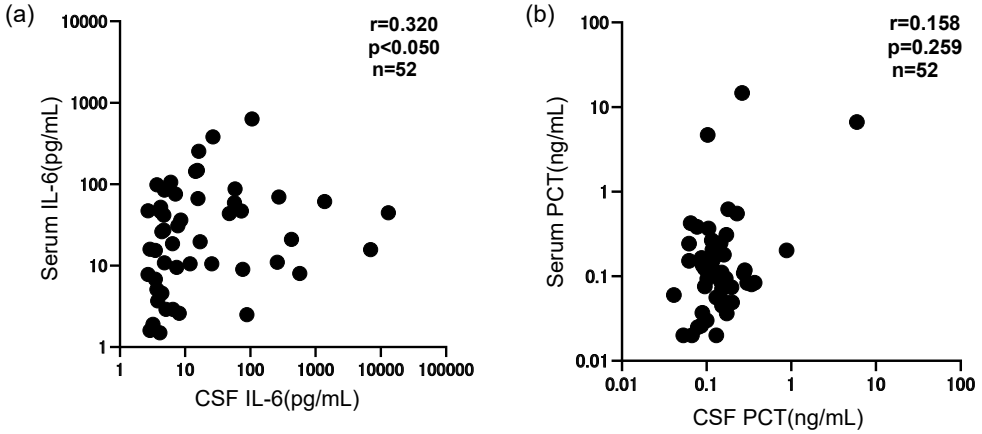

Figure 3 Correlations between IL-6 or PCT concentrations in the CSF and serum. Correlations between IL-6 or PCT concentrations in the CSF and serum are shown (n=52).
CSF, cerebrospinal fluid; IL-6, interleukin-6; PCT, procalcitonin.

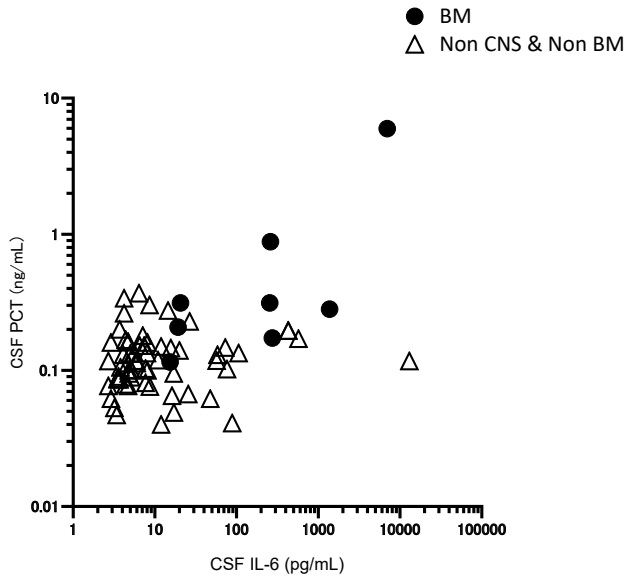

Figure 4 Distribution of participants according to the IL-6 and PCT concentrations in the CSF.
The distribution of participants in the BM group (n=70) according to their CSF IL-6 and CSF PCT concentrations are shown.
CSF, cerebrospinal fluid; IL-6, interleukin-6; PCT, procalcitonin; BM, bacterial meningitis; non-BM, non-bacterial central nervous system diseases

result is consistent with that of the study on the differentiation between BM and aseptic meningitis by Pinto Junior et al. [18]. Diseases other than BM in which elevated CSF IL-6 levels have been reported include viral meningitis, encephalitis, encephalopathy, and cerebral infarction [18),19)-22)]. In the present study, the non-BM group included three cases of viral meningitis, five cases of encephalitis /encephalopathy, and three cases of cerebral infarction, which likely contributed to the observed elevation. (Supplementary **Table1**) The increase in CSF IL-6 levels is thought to be due to an inflammatory response.

In recent years, several studies have investigated the role of CSF PCT and IL-6 in the diagnosis of neonatal and pediatric meningitis. For example, Borowiak et al. reported that CSF PCT and lactate levels have significant diagnostic utility in neonatal meningitis [23]. Similarly, Babenko et al. demonstrated that PCT and C-reactive protein measurements could aid in effectively differentiating BM from enteroviral meningitis in children, using a decision tree approach [24]. Rajial et al. further evaluated the utility of serum and CSF PCT for diagnosing neonatal meningitis, emphasizing its role in differentiating bacterial etiologies from viral etiologies [25]. Furthermore, Kruthika et al. conducted a systematic review of IL-6 as a biomarker for diagnosing tuberculous meningitis, highlighting its potential application in bacterial infections [26]. These findings support the relevance of CSF IL-6 and PCT in various types of meningitis and suggest that their combined measurement may improve the diagnostic accuracy. The low specificity of CSF IL-6 for diagnosing BM compared with other biomarkers (**Table 2**) is likely because of its lack of disease specificity. Although elevated CSF IL-6 concentration alone may lack specificity, it could still be useful as a screening marker for CNS diseases.

To supplement the specificity of CSF IL-6, we focused on PCT, a biomarker known to specifically increases during bacterial inflammation. Previous studies have shown the utility of CSF PCT for diagnosing BM [12)-15)]. In our study, we confirmed the usefulness of CSF PCT levels in patients with BM (**Fig. 1(b)**). CSF PCT levels were not significantly correlated with serum PCT levels (**Fig. 3(b)**), indicating that CSF PCT may have a different dynamic to serum PCT. However, Reshi et al. suggested that during infection, the blood–brain barrier may be disrupted, allowing serum PCT to enter the CSF; therefore, this possibility must be considered. The sensitivity and specificity of CSF PCT levels alone were consistent with those reported by Reshi et al., who reported a sensitivity of 0.92 and specificity of 0.87 [27]. Additionally, the AUC for CSF PCT was higher than that for CSF IL-6 or CSF cell counts for diagnosing BM (**Fig. 2**). The significant difference between the BM and non-BM groups (**Fig. 1(b)**) suggests that the CSF PCT has a high sensitivity for diagnosing BM. This is likely because IL-6 levels increase nonspecifically in inflammatory diseases, whereas PCT levels increase specifically in bacterial inflammation. The elevated CSF PCT levels in patients with BM may be because of the release of PCT from bacteria or leukocytes in the CNS. However, in the present study, elevated CSF PCT levels were also observed in the non-BM group. Raddant and Russo further reported that PCT can be produced by the trigeminal nerve or glial cells during inflammation, leading to a localized increase in the CSF levels [28]. Although we could not elucidate the reason for the elevated CSF PCT levels in the non-BM group, this must be considered when using CSF PCT as a biomarker.

Next, we examined the clinical utility of simultaneous measurement of CSF IL-6 and PCT levels. As shown in **Fig. 4** and **Table 2**, compared with the sensitivity and specificity of CSF IL-6 or PCT alone, when both markers were above their respective cutoff values, the sensitivity was similar or slightly decreased; however, the specificity was significantly improved. In the present study, 26 patients had CSF IL-6 levels above the cutoff, of whom 20 were from groups other than the non-CNS group. Pre-

Table 2 Sensitivity and specificity results of the different parameters

	Sensitivity	Specificity
CSF IL-6	1.00	0.71
CSF PCT	0.88	0.82
CSF cells	0.75	0.74
CSF IL-6 and CSF PCT	0.88	0.95
CSF IL-6 and CSF cells	0.88	0.89
CSF cells and CSF PCT	0.75	0.95

CSF, cerebrospinal fluid; IL-6, interleukin-6; PCT, procalcitonin

vious reports have indicated that patients with CSF IL-6 levels above the cutoff are highly likely to have some form of inflammatory response within the CNS [18]. This is likely the reason for the reduced specificity for diagnosing BM. Of the 26 patients with CSF IL-6 levels above the cutoff, 10 had CSF PCT levels above the cutoff, of which 7 were patients with BM. In one case within the BM group, both CSF IL-6 and CSF PCT levels did not exceed the respective cut-off values. This patient had postoperative meningitis and had received antibiotic therapy prior to CSF sampling, which may have influenced the biomarker concentrations.Conversely, three cases outside the BM group showed biomarker levels above the cut-off values: two cases of encephalitis/encephalopathy and one case of crowned dens syndrome. Because the number of these cases was limited, we were unable to further analyze the underlying reasons for the elevated values.

These results suggest that simultaneous measurements of CSF IL-6 and PCT levels can help identify the presence of CNS disease via CSF IL-6 levels and determine whether the disease is bacterial in origin via CSF PCT levels. This combination compensated for the shortcomings of each marker, resulting in a significant improvement in specificity, although the sensitivity was slightly decreased.

Although the number of patients with BM in this study was small, the above results suggest that the combination of CSF IL-6 and PCT measurements may serve as a useful quantitative biomarker for detecting BM in clinical settings. Further prospective studies with larger patient populations are required to validate the usefulness of these biomarkers, as this study has several limitations. First, as this was a single-center study, there was an inherent risk of bias related to the study design, including the patient selection criteria and data collection methods. Second, the relatively small sample size, particularly the limited number of CSF culture-positive cases in the BM group, may have introduced selection bias, potentially influencing the generalizability of our findings. Moreover, regression analysis could not be performed owing to the small sample size and limited available resources. Third, the study population was limited to patients from a specific medical institution, which may restrict the applicability of our results to different populations, including those from different geographic regions and those with varying disease prevalence rates. Furthermore, measurement of IL-6 and PCT in CSF is currently not covered by the healthcare insurance system in our country. Although there are cost limitations, we believe that their utility as rapid, minimally invasive biomarkers for distinguishing BM from non-CNS conditions justifies consideration, particularly when early differentiation is clinically crucial. Moreover, we hope that similar studies at other institutions, inspired by our research, will help to further validate and enhance the clinical utility of these biomarkers.

V. Conclusion

In conclusion, the combination of CSF IL-6 and PCT measurements provides superior diagnostic accuracy for BM than either marker alone. To further enhance the reliability of these findings, future studies should incorporate regression analyses to adjust for potential confounding factors and to better understand the independent contributions of CSF IL-6 and CSF PCT in BM diagnosis. Additionally, large-scale, multicenter, prospective studies are required to confirm these results across diverse populations and clinical settings. Investigating the impact of different clinical parameters, such as underlying conditions or disease severity, on biomarker performance will also be important for optimizing their clinical application.

Acknowledgements

The authors have no acknowledgements to declare. The research did not receive any specific grant.

Authors' contributions

Takuya Shimura: Conceptualized the research theme, designed the study protocol, conducted the research, and wrote the manuscript. Led most aspects of the study; Hitomi Sakata: Conceptualization, Supervision, Writing - Review & Editing; Masahiro Yamamoto: Writing - Review & Editing; Ryunosuke Ohkawa: Writing - Review & Editing; Akira Yoshimoto: Writing - Review & Editing; Tomonori Suzuki: Writing - Review & Editing; Masato Nishioka: Conceptualization, Supervision, Writing - Review & Editing.

Conflicts of interests

The authors of the study have nothing to disclose.

Data statement

The datasets generated or analyzed during this study are available from the corresponding author upon reasonable request.

References

1) van de Beek D, Cabellos C, Dzupova O, et al. ESCMID guideline: diagnosis and treatment of acute bacterial men-

ingitis. Clin Microbiol Infect. 2016; 22 Suppl 3: S37-62. doi: 10.1016/j.cmi.2016.01.007.

2) van de Beek D, de Gans J, Spanjaard L, et al. Clinical features and prognostic factors in adults with bacterial meningitis. N Engl J Med. 2004; 351: 1849-59. doi: 10.1056/NEJMoa040845.

3) Borhani-Haghighi A, Kardeh B, Banerjee S, et al. Neuro-Behçet's disease: an update on diagnosis, differential diagnoses, and treatment. Mult Scler Relat Disord. 2020; 39: 101906. doi: 10.1016/j.msard.2019.101906.

4) Tanaka T, Narazaki M, Masuda K, et al. Regulation of IL-6 in immunity and diseases. Adv Exp Med Biol. 2016; 941:79-88. doi: 10.1007/978-94-024-0921-5_4.

5) Fujihara K, Bennett JL, de Seze J, et al. Interleukin-6 in neuromyelitis optica spectrum disorder pathophysiology. Neurol Neuroimmunol Neuroinflamm. 2020; 7(5): e841. doi: 10.1212/NXI.0000000000000841.

6) Pandolfi F, Franza L, Carusi V, et al. Interleukin-6 in rheumatoid arthritis. Int J Mol Sci. 2020; 21(15): 5238. doi: 10.3390/ijms21155238.

7) Akman-Demir G, Tüzün E, Içöz S, et al. Interleukin-6 in neuro-Behçet's disease: association with disease subsets and long-term outcome. Cytokine. 2008; 44(3): 373-6. doi: 10.1016/j.cyto.2008.09.003.

8) Wei Y, Chang H, Li X, et al. Cytokines and tissue damage biomarkers in first-onset neuromyelitis optica spectrum disorders: significance of interleukin-6. Neuroimmunomodulation. 2018; 25(4): 215-24. doi: 10.1159/000492543.

9) Kossmann T, Hans VH, Imhof HG, et al. Intrathecal and serum interleukin-6 and the acute-phase response in patients with severe traumatic brain injuries. Shock. 1995; 4(4): 311-7. doi: 10.1097/00024382-199510000-00001.

10) Russwurm S, Wiederhold M, Oberhoffer M, et al. Molecular aspects and natural source of procalcitonin. Clin Chem Lab Med. 1999; 37(8): 789-97. doi: 10.1515/CCLM.1999.111.

11) Samsudin I, Vasikaran SD. Clinical utility and measurement of procalcitonin. Clin Biochem Rev. 2017; 38(2): 59-68. https://www.ncbi.nlm.nih.gov/pmc/articles/PMC5549590/.

12) Magrini L, Gagliano G, Travaglino F, et al. Comparison between white blood cell count, procalcitonin and C reactive protein as diagnostic and prognostic biomarkers of infection or sepsis in patients presenting to emergency department. Clin Chem Lab Med. 2014; 52(10): 1465-72. doi: 10.1515/cclm-2014-0219.

13) Alons IM, Verheul RJ, Kuipers I, et al. Procalcitonin in cerebrospinal fluid in meningitis: a prospective diagnostic study. Brain Behav. 2016; 6(11): e00545. doi: 10.1002/brb3.545.

14) Kepa L, Oczko-Grzesik B, Błedowski D. Procalcitonin (PCT) concentration in cerebrospinal fluid and plasma of patients with purulent and lymphocytic meningoencephalitis--own observations. Przegl Epidemiol. 2005; 59(3): 703-9. https://pubmed.ncbi.nlm.nih.gov/16433332/.

15) Wang H, Zhou C, Fu Y. Factors influencing procalcitonin in the cerebrospinal fluid of patients after neurosurgery and its diagnostic value for intracranial infection. BMC Neurol. 2023; 23(1): 288. doi: 10.1186/s12883-023-03339-8.

16) Prasad R, Kapoor R, Srivastava R, et al. Cerebrospinal fluid TNF-α, IL-6, and IL-8 in children with bacterial meningitis. Pediatr Neurol. 2014(1); 50: 60-5. doi: 10.1016/j.pediatrneurol.2013.08.016.

17) Dano ID, Sadou H, Issaka B, et al. Measurement of interleukin-6 in cerebrospinal fluid for the diagnosis of bacterial meningitis. Pak J Biol Sci. 2016; 19(4): 185-90. doi: 10.3923/pjbs.2016.185.190.

18) Pinto Junior VL, Rebelo MC, Gomes RN, et al. IL-6 and IL-8 in cerebrospinal fluid from patients with aseptic meningitis and bacterial meningitis: their potential role as a marker for differential diagnosis. Braz J Infect Dis. 2011; 15(2): 156-8. doi: 10.1590/s1413-86702011000200011.

19) Liu DB, Zhang HP, Yu K, et al. A study on correlations of procalcitonin and interleukin-6 with viral meningitis. Eur Rev Med Pharmacol Sci. 2018; 22(11): 3474-8.

20) Fujimori J, Takahashi T, Kaneko K, et al. Anti-NMDAR encephalitis may develop concurrently with anti-MOG antibody-associated bilateral medial frontal cerebral cortical encephalitis and relapse with elevated CSF IL-6 and CXCL13. Mult Scler Relat Disord. 2021; 47: 102611. doi: 10.1016/j.msard.2020.102611.

21) Bodro M, Compta Y, Llansó L, et al. Increased CSF levels of IL-1 β , IL-6, and ACE in SARS-CoV-2-associated encephalitis. Neurol Neuroimmunol Neuroinflamm. 2020; 7(5): e821. doi: 10.1212/NXI.0000000000000821.

22) Virupakshaiah A, Moseley CE, Elicegui S, et al. Life-threatening MOG antibody-associated hemorrhagic ADEM with elevated CSF IL-6. Neurol Neuroimmunol Neuroinflamm. 2024; 11(4): e200243. doi: 10.1212/NXI.0000000000200243.

23) Borowiak A, Safranow K, Sarna A, et al. Diagnostic utility of procalcitonin and lactate determination in cerebrospinal fluid for the diagnosis of neonatal meningitis. J Clin Med. 2025; 14(2): 414. doi: 10.3390/jcm14020414.

24) Babenko D, Seidullayeva A, Bayesheva D, et al. Ability of procalcitonin and C-reactive protein for discriminating between bacterial and enteroviral meningitis in children using decision tree. Biomed Res Int. 2021; 2021: 5519436. doi: 10.1155/2021/5519436.

25) Rajial T, Batra P, Harit D, et al. Utility of cerebrospinal fluid and serum procalcitonin for the diagnosis of neonatal meningitis. Am J Perinatol. 2022; 3(4)9: 373-8. doi: 10.1055/s-0040-1716406.

26) Kruthika P. Role of IL-6 as a biomarker in the diagnosis of

tuberculous meningitis - A systematic review. Int J Mycobacteriol. 2022; 11(3): 229-35. doi: 10.4103/ijmy.ijmy_101_22.
27) Reshi Z, Nazir M, Wani W, et al. Cerebrospinal fluid procalcitonin as a biomarker of bacterial meningitis in neonates. J Perinatol. 2017; 37(8): 927-31. doi: 10.1038/jp.2017.73.
28) Raddant AC, Russo AF. Reactive oxygen species induce procalcitonin expression in trigeminal ganglia glia. Headache. 2014; 54: 472-84. doi: 10.1111/head.12301

Review Article

DSS1 in clinical laboratory medicine and oncology from RNA metabolism and R-loop homeostasis to BRCAness and PARP inhibitor response

†Yasuhiro Sakai[*1,2], *Kazuhiko Kuwahara*[*3], *Masatomo Kimura*[*3,4], *Hiroyasu Ito*[*1]

†Correspondence: Department of Joint Research Laboratory of Clinical Medicine, Fujita Health University School of Medicine, 1-98 Dengakugakubo, Kutsukake, Toyoake, Aichi 470-1192, Japan
Tel: +81-562-93-2319 ; Fax: +81-562-95-3761
E-mail: ya-sakai@fujita-hu.ac.jp
Received January 20, 2026; accepted March 28, 2026
*1 Department of Joint Research Laboratory of Clinical Medicine, Fujita Health University School of Medicine, Aichi, Japan
*2 Department of Tumor Pathology, Hamamatsu University School of Medicine, Shizuoka, Japan
*3 Department of Pathology, Kindai University Faculty of Medicine, Osaka, Japan
*4 Department of Diagnostic Pathology, Hashimoto Municipal Hospital, Wakayama, Japan

ABSTRACT

Cancer genome testing routinely reports driver alterations, mutational signatures, and DNA repair states, yet key clinical phenotypes—tumor behavior, relapse risk, and chemoresistance—are not fully explained by genotype alone. Deleted in split-hand/split-foot 1 (DSS1) is a small, acidic, intrinsically disordered protein conserved across eukaryotes and shared by several large multiprotein assemblies, making it a plausible functional modifier of these phenotypes. This review summarizes DSS1 biology from the perspective of clinical laboratory medicine, focusing on how DSS1 links RNA metabolism, R-loop homeostasis, and homologous recombination repair (HRR) and how this linkage may inform biomarker development. Mechanistically, DSS1 behaves as a stabilizing "molecular glue" in protein complexes and serves as a core component of RNA export/quality-control modules, including TREX-2 and the TREX-2.1/REX complex, which regulate co-transcriptional messenger ribonucleoprotein remodeling, nuclear export, and RNA surveillance—processes closely tied to R-loop (DNA:RNA hybrid) control and transcription-coupled DNA damage. DSS1 is also an obligate cofactor of BRCA2: DSS1 binding stabilizes BRCA2, improves its solubility, and limits off-target interactions, supporting repair-competent BRCA2 in the nucleus. We then review clinicopathological evidence that DSS1 dysregulation correlates with cancer behavior, including shorter relapse-free survival and a chemoresistant phenotype. Finally, we propose that DSS1-low, *BRCA*-proficient tumors may acquire BRCAness, providing a rationale for PARP inhibitor responses beyond current BRCA-focused companion diagnostics, and we outline how standardized DSS1 measurement (mRNA and/or protein), integrated with BRCA status and other HRR-related signatures, could refine molecular testing and therapeutic stratification in routine practice.

〔Lab Med Int 2026; 5(2): 67-77〕

Key Words
BRCAness, DSS1, PARP inhibitor, R-loop, transcription-coupled DNA damage

I. Introduction

Cancer genome testing has transformed oncology from descriptive histology to molecular pathology by reading out driver alterations, mutational signatures, and repair-pathway states. These readouts reflect multiple mutagenic and repair processes and illustrate not only oncogenic mechanisms but also actionable alterations that predict chemosensitivity[1)2)]. To interpret them further, we need to map each alteration onto its

underlying oncogenic pathway. Some alternative patterns come from outside exposures (e.g., UV light or tobacco), while others are caused by enzymatic mutagenesis (e.g. activation-induced cytidine deaminase (AID) / apolipoprotein B mRNA editing catalytic polypeptide-like (APOBEC) family), mismatch-repair failure, or replication stress[3)4)]. In some contexts, transcription itself may also add DNA damage both controllably and pathologically, the latter of which is called transcription-coupled DNA damage[5)6)].

Deleted in split-hand/split-foot 1 (DSS1) was originally described through genetic mapping studies of split-hand/split-foot malformation (SHFM), where it appeared within a critical chromosomal region on 7q21.3–q22.17). However, the developmental abnormalities in SHFM are now more commonly attributed to dysregulation of genes near DSS1, such as DLX5 and DLX6, than to a DSS1-specific mechanism[8)]. Subsequent biochemical and genetic analyses revealed that DSS1 is a highly conserved, small (~70 amino acids in yeast; ~70–80 in mammals), acidic, and intrinsically disordered protein with surprisingly broad functional diversity[7)9)–12)].

Orthologs of DSS1, termed Sem1 in budding yeast, are conserved across eukaryotes[10)13)]. DSS1/Sem1 is now recognized as a component of multiple large protein complexes, including the 19S lid of the 26S proteasome, a stable subunit of the TRanscription–EXport-2 (TREX-2) and TREX-2.1/Repressor of EXport (REX) complexes, and an essential cofactor of BRCA2 in homologous recombination (HR)[14)–22)]. Therefore, DSS1 contributes to several fundamental processes: protein degradation, mRNA biogenesis and export, transcription-coupled genome maintenance, DNA repair, and replication stress responses. Accordingly, genetic and functional alterations in DSS1 or its partner complexes can affect genomic instability, oncogenesis, chemoresistance, and tumor development[23)–29)].

Here, we review DSS1 from the perspective of clinical laboratory medicine. We first outline its molecular and structural properties, as well as its role as an obligate cofactor of BRCA2 in HR and R-loop control. We then summarize clinicopathological and experimental evidence linking DSS1 dysregulation to cancer behavior. Finally, we show the emergence of BRCAness and poly (adenosine diphosphate-ribose) polymerase inhibitor (PARPi) sensitivity in DSS1-low, *BRCA*-proficient tumors, and discuss how DSS1 could be developed as a biomarker and therapeutic modifier in cancer genome testing.

II. Structural and functional roles of DSS1

Molecular and structural features of DSS1

The human DSS1 gene is located on chromosome 7q21 and encodes a small acidic protein of ~70 amino acids[7)13)]. Orthologous genes (Sem1 in *Saccharomyces cerevisiae, dss1*$^{+}$ in *Schizosaccharomyces pombe*, etc.) show strong sequence conservation of acidic and hydrophobic motifs[11)13)30)]. DSS1 lacks extensive secondary structure under physiological conditions, being classified as an intrinsically disordered protein[31)32)]. Nuclear magnetic resonance spectroscopy and other biophysical analyses indicate that DSS1 can transiently form helical segments and multiple short linear motifs, which become stabilized upon binding to structured partners[33)34)].

This intrinsic disorder gives DSS1 two key properties: 1) binding plasticity, allowing DSS1 to interact with numerous partners through distinct interfaces, and 2) molecular "glue" behavior, whereby DSS1 often binds at the interface between two or more structured subunits and stabilizes their assembly. Small, acidic, intrinsically disordered proteins such as DSS1 function as molecular glues in the PCI-containing complexes, inserting between PCI domain proteins to stabilize and regulate large multiprotein assemblies[11)12)17)]. Comprehensive interactome analyses, particularly in *S. pombe*, have revealed that DSS1 associates with a broad range of complexes, including the 19S lid of the 26S proteasome, the TREX-2 and TREX-2.1/REX complexes, the Thp3–Csn12–Sem1 complex, and mitotic septin assemblies[14)-22)35)]. This diversity suggests that DSS1 functions more as a general scaffolding cofactor for PCI-containing complexes than as a single-pathway factor. In addition, DSS1 forms an obligate complex with the non-PCI tumor suppressor BRCA2[13)].

DSS1 in the TREX-2 complex, mRNA nuclear export, and R-loop formation

The TREX-2 complex is a conserved assembly that couples transcription to mRNA export at the nuclear pore complex (NPC). In mammals, TREX-2 is built on a germinal center–associated nuclear protein (GANP) scaffold, with DSS1, PCI domain–containing 2 (PCID2), enhancer of yellow 2 (ENY2), and centrin 2/3 (CETN2/3) as additional subunits (**Figure 1**)[18)19)22)]. TREX-2 interacts with the NPC and transcriptional regulators (e.g., mediator), thereby facilitating the delivery of nascent transcripts to nuclear pores[36)-38)]. In yeast, Sem1-deficient cells show defective mRNA export, impaired transcription elongation, and accumulation of

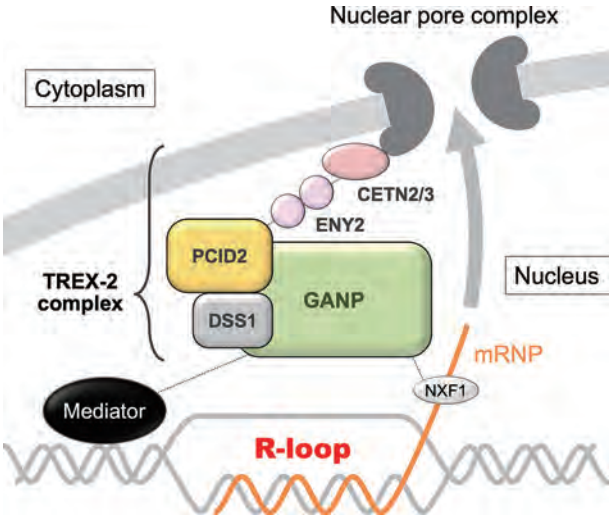

Figure 1 Schematic representation of mRNA nuclear export through the nuclear pore complex. In mammals, the TRanscription–EXport-2 (TREX-2) complex comprises germinal center–associated nuclear protein (GANP), deleted in split-hand/split-foot 1 (DSS1), PCI domain–containing 2 (PCID2), enhancer of yellow 2 (ENY2), and centrin 2/3 (CETN2/3). TREX-2 associates with messenger ribonucleoprotein (mRNP) particles, in part via the mRNA export receptor nuclear RNA export factor 1 (NXF1), and facilitates the targeting of transcripts to nuclear pores for export to the cytoplasm. Impaired TREX-2 function can lead to nuclear retention of mRNA and is proposed to increase the opportunity for nascent RNA to re-anneal to its template DNA, forming DNA:RNA hybrids (R-loops). Excessive or persistent R-loops can promote transcription-associated DNA damage, including replication stress and DNA double-strand breaks, and thereby contribute to mutagenesis and genome instability. Adapted from Pathol Int 2024; 74(3): 103–18 with permission and minor modification[19].

DNA damage; this phenotype is similar to that of cells lacking other TREX-2 components or the principal mRNA export receptor Mex67/nuclear RNA export factor 1 (NXF1)[26)39)-42)]. In mammals, DSS1/Sem1 is similarly included in the TREX-2 complex, although its dynamics may vary among cell types or conditions.

TREX-2 is now recognized as an important factor in R-loop homeostasis. R-loops are three-stranded structures that form when the nascent RNA transcript slips back and re-anneals to its DNA template, creating a DNA:RNA hybrid and leaving the non-template DNA strand displaced as a single-stranded DNA (ssDNA). R-loops can have useful functions under physiological conditions. They form at certain promoters and transcription terminator regions, where they help control transcription initiation and termination and influence local chromatin structure[43)-47)]. In B cells, R-loops at immunoglobulin switch regions are deliberately formed as intermediates of class-switch recombination, because the exposed ssDNA is targeted by AID to trigger programmed DNA breakage and joining[48)-51)]. In other systems, including mitochondrial DNA, R-loop-like structures contribute to replication initiation by providing both an RNA primer and a structural platform for DNA polymerases[52)-55)]. In these contexts, R-loops are formed at specific loci and removed once their role is fulfilled, maintaining what is often referred to as R-loop homeostasis.

However, when R-loops become too abundant, too stable, or mislocalized, they turn from useful intermediates into threats to genome integrity. Persistent R-loops act as roadblocks for replication forks, leading to fork stalling, reversal, or collapse, and thereby causing replication stress and DNA double-strand breaks (DSBs)[56)-59)]. The displaced ssDNA is chemically vulnerable and prone to damage and erroneous repair; therefore, excessive R-loops drive mutagenesis and are recognized as a major source of transcription-coupled DNA damage[60)-62)]. Factors that play a role in RNA processing and export, helicases that unwind DNA:RNA hybrids, and topoisomerases that relieve torsional stress help prevent harmful R-loop accumulation; when these systems fail, R-loops build up and contribute to oncogenesis[63)-65)].

The TREX-2 complex is positioned at the nuclear pore, where it helps move nascent RNA transcripts away from their template DNA by anchoring actively transcribed genes near the pore basket and handing the transcripts off to the export receptor NXF1[38)66)-68)]. By reducing the dwell time of free RNA near its template DNA, the TREX-2 complex is thought to lower the chance that RNA will re-anneal and form R-loops. Collectively,

the TREX-2 complex may promote co-transcriptional messenger ribonucleoprotein (mRNP) remodeling and efficient export. Although the exact contribution of DSS1 within the TREX-2 complex to R-loop suppression remains incompletely defined, DSS1 deficiency may impair TREX-2 function and thus indirectly promote R-loop accumulation and transcription-coupled DNA damage.

DSS1 in the TREX-2.1/REX complex

DSS1 also plays a key role in the human TREX-2.1 complex, which was recently described[21]. The TREX-2.1 complex is a trimer composed of LENG8, DSS1, and PCID2: LENG8 and PCID2 are PCI domain proteins, and DSS1 binds their PCI-type helical scaffolds in the same way as in GANP–PCID2 of the TREX-2 complex. Structural studies show that the TREX-2.1 complex binds the DEAD-box helicase DDX39B (UAP56), a core component of another mRNA nuclear export machinery, the THO/TREX complex.

Functionally, the TREX-2.1 complex behaves as an mRNP remodeling factor that controls DDX39B activity. Biochemical studies have shown that the TREX-2.1 complex binds directly to DDX39B, stimulates its ATPase activity, and can displace it from RNA[21]. More recently, the same LENG8–DSS1–PCID2 module has been identified as the core of the REX complex, which acts in nuclear RNA quality control. In that pathway, LENG8 is recruited to incompletely processed or intron-retaining transcripts and targets them for degradation instead of allowing them to be exported from the nucleus[21,69]. Together, these findings indicate that DSS1 is an essential factor in RNA metabolism, including post-splicing control, mRNA nuclear export, and nuclear RNA surveillance. However, whether DSS1-driven abnormalities in RNA processing directly contribute to oncogenesis remains unclear.

DSS1 as an obligatory cofactor of BRCA2 in homologous recombination

When a DNA DSB occurs, the sister chromatid serves as a template for the homologous recombination repair (HRR) pathway. BRCA2 is an important HRR factor that loads RAD51 recombinase onto ssDNA at DSBs and stalled replication forks[70-72]. DSS1 forms a stable complex with the BRCA2 DNA-binding domain (DBD) and is considered an obligate partner of BRCA2[13,73]. Biochemical and structural studies show that DSS1 binds to multiple surfaces of the BRCA2 DBD, including the helical domain and the oligonucleotide/oligosaccharide-binding (OB) folds[25,73]. This interaction stabilizes BRCA2, improves its solubility, and promotes efficient RAD51 filament formation on ssDNA. DSS1 depletion or *BRCA2* mutations that weaken DSS1 binding reduce the steady-state level of BRCA2 in the nucleus, shift it into less-soluble, partially aggregated states, and decrease nuclear HRR activity[23,74-76].

In addition, DSS1 prevents binding of the BRCA2 DBD to double-stranded DNA (dsDNA). In the absence of DSS1, BRCA2 exhibits increased binding to dsDNA, which could misdirect RAD51 to inappropriate regions[25]. Moreover, loss of DSS1 induces aberrant BRCA2 oligomeric states that are less competent for proper RAD51 loading[75,77]. Thus, the BRCA2–DSS1 partnership is essential for maintaining stable, correctly assembled, repair-competent BRCA2 molecules in the nucleus (**Figure 2**). This tuning mechanism provides a useful conceptual framework: DSS1 acts as an allosteric

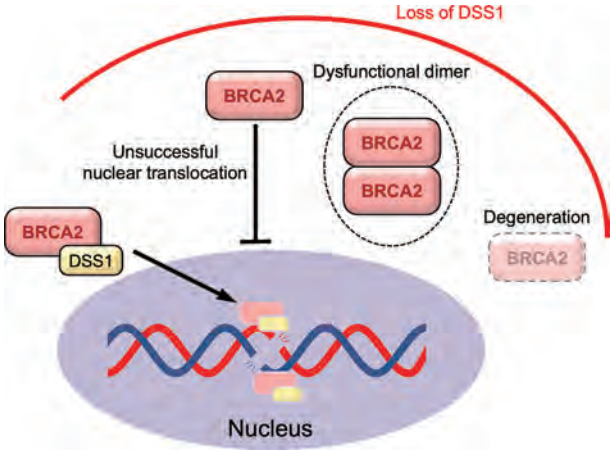

Figure 2 Schematic representation of BRCA2 dysfunction in the absence of DSS1. Loss of DSS1 destabilizes BRCA2, leading to altered nuclear distribution, formation of aberrant and nonfunctional BRCA2 dimers/oligomers, and BRCA2 degradation mediated by chaperones.

modulator that optimizes BRCA2's substrate specificity in HRR and replication fork protection while reducing off-target interactions that could be deleterious.

BRCA2 also participates in R-loop processing. Several observations suggest that BRCA2 helps prevent harmful R-loop accumulation. BRCA2 interacts with RNA polymerase II and factors that control promoter-proximal pausing, and thereby helps avoid prolonged stalling of the transcription machinery, a situation that favors R-loop formation[78)79)]. In addition, BRCA2 works together with R-loop–processing factors such as the RNA helicase DDX5 and the ribonuclease RNase H2 to dissolve DNA:RNA hybrids and repair R-loop–associated lesions[79)80)]. Moreover, interactions between BRCA2 and subunits of the TREX-2 complex help suppress R-loop–induced genomic instability[81)].

Thus, it is plausible that DSS1, by jointly acting in the TREX-2 complex and BRCA2, coordinates mRNA metabolism with HR-mediated processing.

III. DSS1 dysregulation in breast cancer

Our work and that of others have examined DSS1 expression in human cancers[27)-29)]. Because DSS1 participates in mRNA metabolism, R-loop homeostasis, and HRR machinery, its dysfunction is thought to be closely associated with oncogenesis and chemosensitivity in various cancers.

Of all cancer types, the association between DSS1 expression and breast cancer has been examined most thoroughly. We have reported that, in invasive breast carcinomas, high DSS1 expression was associated with significantly shorter relapse-free survival although the DSS1 level did not correlate strongly with classical clinicopathological factors such as tumor size, nodal status, histological grade, hormone receptor status, or Ki-67 index[27)]. This indicates that DSS1 is an independent marker that is not simply a surrogate for proliferation or advanced stage. Interestingly, functional assays using breast cancer cell lines complemented the clinical data[27)]. DSS1-overexpressing MCF7 cells (estrogen receptor α (ERα)-positive, p53 wild type) showed decreased chemosensitivity to DNA-damaging agents such as camptothecin and etoposide. Cell-cycle analysis and apoptosis assays showed that these cells had a smaller sub-G1 fraction after drug exposure than control cells, indicating increased chemoresistance. Conversely, siRNA-mediated DSS1 knockdown suppressed proliferation and induced apoptosis in both MCF7 and drug-resistant MDA-MB-231 (triple-negative, p53-deficient) cells. When combined with camptothecin or etoposide, DSS1 knockdown further enhanced drug-induced cell death, particularly in MDA-MB-231 cells.

Another study of ours extended these findings by analyzing DSS1 together with PCID2 and BRCA2 in breast carcinomas. DSS1 expression was consistently higher in tumor tissues than in normal breast tissue, whereas PCID2 expression was similar between normal and malignant tissues (**Figure 3**)[28)]. When patients were divided into high- and low-expression groups for DSS1, BRCA2, and PCID2, only DSS1 showed a significant association with poor relapse-free survival. This confirmed DSS1 as the key clinical predictor among these three factors. In vitro analysis, propidium iodide staining, single-cell gel electrophoresis (comet assays), and clonogenic survival assays to assess chemosensitivity revealed that DSS1 depletion in breast cancer cell lines increased sensitivity to several DNA-damaging agents, whereas DSS1 overexpression conferred chemoresistance[28)].

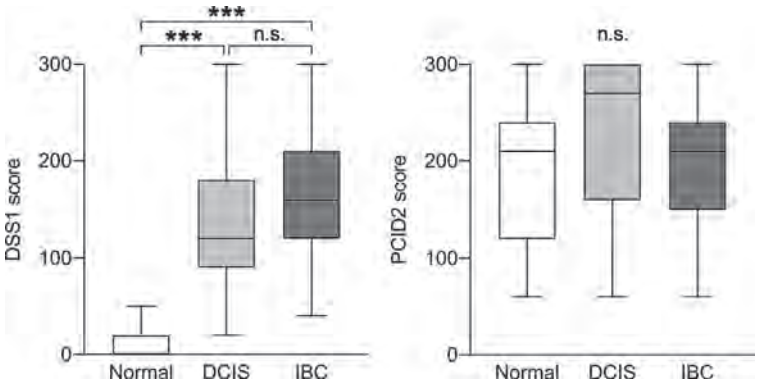

Figure 3 DSS1 (left) and PCID2 (right) expression scores in normal breast tissue, ductal carcinoma in situ (DCIS), and invasive breast carcinoma (IBC). Expression scores (0–300) were calculated by multiplying staining intensity (0–3; weak to strong) by the percentage of positive cells (0%–100%) in immunohistochemistry. Box plots show the median (center line) and the 25th and 75th percentiles (box); whiskers indicate the range. ***$P < 0.001$; n.s., not significant. Adapted from Lab Invest 2021; 101 (8): 1048–59 with permission and minor modification[28)].

Importantly, BRCA2 expression itself did not significantly affect chemosensitivity under the same conditions, even though DSS1 depletion reduced BRCA2 protein levels. This indicates that the change in drug response after DSS1 knockdown is not simply a consequence of reduced BRCA2. Furthermore, PCID2 behaved similarly to DSS1 at the functional level.

Taken together, DSS1 is a clinically relevant modifier of breast cancer behavior that sits squarely within the scope of clinical laboratory medicine. Functional data revealed that high DSS1 is not just a passive marker but a surrogate for a tumor's ability to tolerate genotoxic stress, whereas low DSS1 defines a potentially druggable vulnerability. For clinical laboratory medicine, this means that DSS1 expression is a candidate prognostic and predictive biomarker that could, after further validation, be incorporated alongside ER, progesterone receptor (PR), human epidermal growth factor receptor 2 (HER2), Ki-67, and p53 to refine risk stratification and anticipate response to standard chemotherapy.

IV. DSS1 dysregulation in renal cancer

The work of others has indicated that DSS1 is upregulated in metastatic clear cell renal cell carcinoma (ccRCC) and promotes both primary tumor growth and metastasis[29]. High DSS1 expression correlates with a gene signature of proliferation and with poorer outcomes in renal cancer datasets. In addition, large-scale CRISPR screening has identified DSS1 among genes that are essential for the survival of many ccRCC cell lines, suggesting that ccRCC cells depend on DSS1 for fitness.

In metastatic ccRCC cell lines and mouse models, DSS1 promotes tumor growth and lung metastasis[29]. DSS1 interacts directly with LC3 and, via the E3 ligase TRIM25, enhances K63-linked polyubiquitination of LC3B, which leads to suppression of autophagic flux. DSS1 knockdown increases autophagic vacuoles and LC3 puncta, while DSS1 overexpression has the opposite effect, indicating that DSS1 functions as a negative regulator of autophagy in ccRCC. Functionally, when autophagy is restored (by DSS1 silencing or pharmacologic manipulation), ccRCC cells show reduced proliferation, migration, invasion, and metastatic potential. Furthermore, this autophagy block feeds directly into epithelial–mesenchymal transition (EMT) control. DSS1-mediated inhibition of autophagy stabilizes the EMT transcription factor TWIST1, which is otherwise degraded through autophagy.

Overall, DSS1's repertoire may extend beyond genomic maintenance, linking it to autophagy regulation, EMT, and metastatic signaling pathways.

V. BRCAness and PARPi chemosensitivity in DSS1-low cancers

Cancer genome profiling is now indispensable in modern clinical laboratory medicine. In breast, ovarian, and prostate cancers, both hereditary and sporadic

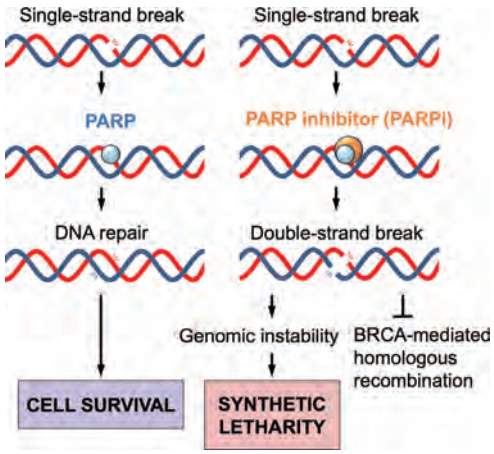

Figure 4 Schematic representation of DNA repair by poly(adenosine diphosphate-ribose) polymerase (PARP) and the basis of PARP inhibitor (PARPi)–induced synthetic lethality. PARP recognizes SSBs and promotes their repair, supporting cell survival. PARPi inhibit PARP activity at SSBs, causing unrepaired lesions to be converted into DNA double-strand breaks (DSBs) during replication. When homologous recombination repair (HRR), including BRCA1/2-dependent pathways, is intact, such DSBs can be repaired; when HRR is defective, DSB repair fails and cell death ensues. Thus, the combination of HRR deficiency and PARP inhibition is expected to selectively kill HR-deficient cells, a phenomenon termed "synthetic lethality." Notably, clinical responses to PARPi have also been observed in subsets of ovarian and prostate cancers without detectable BRCA mutations by current companion diagnostics, suggesting that additional mechanisms beyond canonical BRCA-dependent synthetic lethality may contribute to PARPi sensitivity.

BRCA mutations lead to impaired HRR for DNA damage, contributing to oncogenesis and malignant progression. For such tumors, PARPi have long been expected to exhibit high therapeutic efficacy based on "synthetic lethality." PARPi block the repair of DNA single-strand breaks (SSBs); as a result, in cancer cells that already have defective HRR due to *BRCA* mutations, unrepaired SSBs are converted into DSBs during replication and become essentially irreparable, which selectively kills *BRCA*-mutated cancer cells while largely sparing normal cells (**Figure 4**).

However, recent clinical trials in ovarian and prostate cancers have shown that PARPi can be effective even in patients who test negative on current companion diagnostics for *BRCA* mutations[82)83)]. There is a subset of cancer cells that, despite being *BRCA*-proficient, display biological features similar to *BRCA*-mutated cells—a condition referred to as "BRCAness." Nevertheless, the detailed molecular mechanisms underlying this phenotype, as well as reliable pathological diagnostic methods, have yet to be established.

We therefore hypothesize that, because DSS1 is required for optimal BRCA2 function, DSS1 depletion might disrupt the BRCA2–DSS1 interface and thereby induce BRCAness even in *BRCA2*-proficient cells. We found that, among ovarian cancer subtypes, DSS1 expression was significantly lower in serous carcinoma than in other histological types such as endometrioid, clear cell, and mucinous carcinomas (**Figure 5**). This pattern is consistent with the clinical trial data showing that PARPi are effective in patients with serous carcinoma, irrespective of the results of current companion diagnostics for *BRCA* mutations. In prostate specimens, our small series further suggested that DSS1 expression was generally higher in high-grade prostatic intraepithelial neoplasia (PIN) and appeared to gradually decrease as the Gleason pattern increased from 3 to 5 in acinar adenocarcinomas (**Figure 6**). Functional analyses also indicated that DSS1 depletion reduced HRR activity and enhanced PARPi sensitivity (unpublished data).

Taken together, these observations support a model in which reduced DSS1 expression induces a BRCA-like HRR deficiency and thereby contributes to a BRCAness phenotype that enhances PARPi sensitivity. From the perspective of clinical laboratory medicine, DSS1 expression is therefore a promising biomarker candidate to identify BRCAness in *BRCA*-proficient tumors and to refine the indication for PARPi therapy beyond current BRCA-focused companion diagnostics. In the future, standardized DSS1 assays and integrated interpretation with BRCA status and other HRR-related signatures may help clarify the pathobiology of BRCAness and improve the design of molecular testing panels in routine practice.

VI. Conclusion

From the viewpoint of clinical laboratory medicine, DSS1 is important because it links several key pathways that we already try to assess in daily practice: mRNA metabolism, R-loop homeostasis, HRR activity, replication stress, and even autophagy and EMT in some tumors. Current cancer genome tests mainly tell us what is mutated (for example, BRCA1/2 status or HRR gene

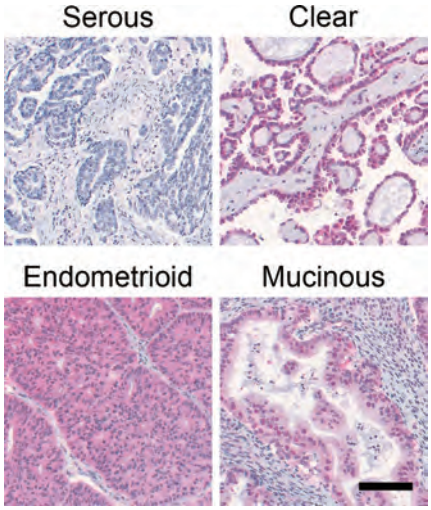

Figure 5 Representative immunohistochemistry for DSS1 in ovarian carcinoma subtypes (unpublished data). DSS1 expression is maintained in clear cell, endometrioid, and mucinous carcinomas, whereas it is reduced in serous carcinoma. Reduced DSS1 expression may destabilize BRCA2 and potentially contribute to a "BRCAness" phenotype. These observations are consistent with clinical trial data showing PARP inhibitor activity in serous ovarian carcinoma beyond current BRCA-focused companion diagnostics.

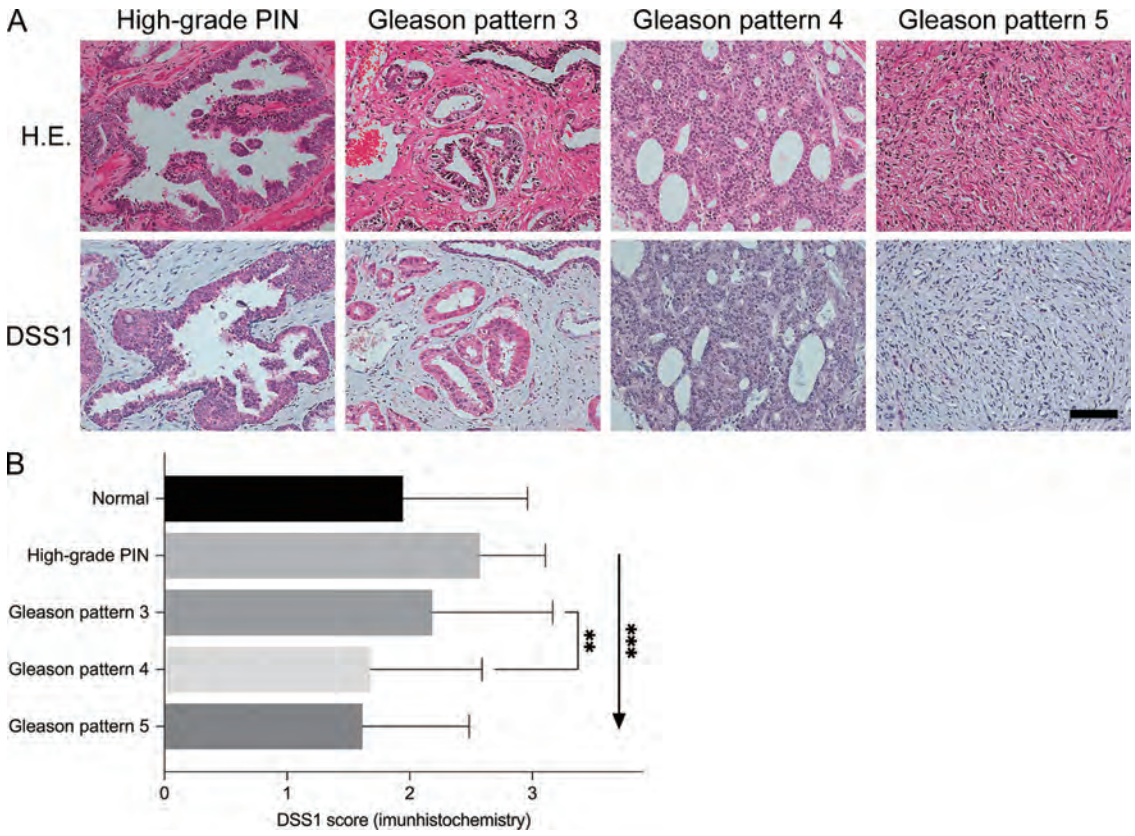

Figure 6 DSS1 expression in prostate cancer (unpublished data). (A) Representative immunohistochemistry for DSS1 across prostatic lesions and Gleason patterns. (B) DSS1 staining is relatively high in high-grade prostatic intraepithelial neoplasia (PIN) and decreases in acinar adenocarcinoma with increasing Gleason pattern (3–5), as assessed by the Cochran–Armitage trend test (***$P < 0.001$). In addition, the Kruskal-Wallis test followed by Dunn's multiple comparison test showed that DSS1 expression in Gleason pattern 4 carcinoma is significantly lower than that in Gleason pattern 3 carcinoma (**$P = 0.003$). These findings suggest that DSS1 expression tends to decline with histologic progression, and that BRCAness may occur in higher-grade prostate cancer.

panels), but they often cannot explain why some *BRCA*-proficient tumors behave as if they were HR-deficient, or why tumors with similar genotypes show very different responses to chemotherapy and PARPi. Because DSS1 is an essential cofactor of BRCA2 and a shared component of TREX-2 and TREX-2.1/REX complexes, its expression and function may provide a more "functional" readout of these pathways.

The next step for clinical laboratories is to turn this concept into practical tools. DSS1 could be measured at the RNA level in NGS panels and at the protein level by immunohistochemistry, and its status could then be interpreted together with *BRCA* mutations, HR deficiency scores, and other markers of transcription- and replication-related DNA damage. Prospective studies that correlate DSS1 status with prognosis and treatment response, especially to PARPi and DNA-damaging regimens, will be crucial. If such data accumulate and assays are standardized, DSS1 has the potential to become a routine biomarker in cancer genome testing—helping us not only to classify tumors, but also to predict which patients truly have BRCAness, which tumors are likely to be chemoresistant, and where new therapeutic vulnerabilities may lie.

Acknowledgments

We would like to thank Profs. Tatsuya Toyama and Seiji Okada for sincere encouragement and supervision of the research projects, and Dr. Krittamate Saisuwan for technical assistance. Yasuhiro Sakai was announced as the winner of the Young Investigator Award in 2024 from the Japanese Society of Laboratory Medicine (JSLM). This work was presented at the 72nd Annual Meeting of the JSLM (held in Chiba, Japan on August 30, 2025) by Yasuhiro Sakai. These studies were supported by JSLM Fund for the Promotion of Scientific Research.

Disclosure of Conflicts of Interest

The authors have no conflicts of interest to declare.

References

1) Alexandrov LB, Nik-Zainal S, Wedge DC, et al. Signatures of mutational processes in human cancer. Nature. 2013; 500(7463): 415-21.
2) Helleday T, Eshtad S, Nik-Zainal S. Mechanisms underlying mutational signatures in human cancers. Nat Rev Genet. 2014; 15(9): 585-98.
3) Burns MB, Temiz NA, Harris RS. Evidence for APOBEC3B mutagenesis in multiple human cancers. Nat Genet. 2013; 45(9): 977-83.
4) Roberts SA, Gordenin DA. Hypermutation in human cancer genomes: footprints and mechanisms. Nat Rev Cancer. 2014; 14(12): 786-800.
5) Santos-Pereira JM, Aguilera A. R loops: new modulators of genome dynamics and function. Nat Rev Genet. 2015; 16(10): 583-97.
6) Gaillard H, Aguilera A. Transcription as a threat to genome integrity. Annu Rev Biochem. 2016; 85: 291-317.
7) Crackower MA, Scherer SW, Rommens JM, et al. Characterization of the split hand/split foot malformation locus SHFM1 at 7q21.3-q22.1 and analysis of a candidate gene for its expression during limb development. Hum Mol Genet. 1996; 5(5): 571-9.
8) Birnbaum RY, Everman DB, Murphy KK, et al. Functional characterization of tissue-specific enhancers in the DLX5/6 locus. Hum Mol Genet. 2012; 21(22): 4930-8.
9) Sowińska-Seidler A, Socha M, Jamsheer A. Split-hand/foot malformation - molecular cause and implications in genetic counseling. J Appl Genet. 2014; 55(1): 105-15.
10) Jäntti J, Lahdenranta J, Olkkonen VM, et al. SEM1, a homologue of the split hand/split foot malformation candidate gene Dss1, regulates exocytosis and pseudohyphal differentiation in yeast. Proc Natl Acad Sci U S A. 1999; 96(3): 909-14.
11) Tomko RJ Jr, Hochstrasser M. The intrinsically disordered Sem1 protein functions as a molecular tether during proteasome lid biogenesis. Mol Cell. 2014; 53: 433-43.
12) Kragelund BB, Schenstrøm SM, Rebula CA, et al. DSS1/Sem1, a multifunctional and intrinsically disordered protein. Trends Biochem Sci 2016; 41(5): 446-59.
13) Marston NJ, Richards WJ, Hughes D, et al. Interaction between the product of the breast cancer susceptibility gene BRCA2 and DSS1, a protein functionally conserved from yeast to mammals. Mol Cell Biol. 1999; 19(7): 4633-42.
14) Sone T, Saeki Y, Toh-e A, et al. Sem1p is a novel subunit of the 26 S proteasome from Saccharomyces cerevisiae. J Biol Chem. 2004; 279(27): 28807-16.
15) Paraskevopoulos K, Kriegenburg F, Tatham MH, et al. Dss1 is a 26S proteasome ubiquitin receptor. Mol Cell. 2014; 56(3): 453-61.
16) Jani D, Lutz S, Hurt E, et al. Functional and structural characterization of the mammalian TREX-2 complex that links transcription with nuclear messenger RNA export. Nucleic Acids Res. 2012; 40(10): 4562-73.
17) Ellisdon AM, Dimitrova L, Hurt E, et al. Structural basis for the assembly and nucleic acid binding of the TREX-2 transcription-export complex. Nat Struct Mol Biol. 2012; 19(3): 328-36.
18) Sakai Y, Phimsen S, Okada S, et al. The critical role of germinal center-associated nuclear protein in cell biology, immunohematology, and hematolymphoid oncogenesis. Exp Hematol. 2020; 90: 30-8.
19) Sakai Y, Kuwahara K. Carcinogenesis caused by transcription-coupled DNA damage through GANP and other components of the TREX-2 complex. Pathol Int. 2024; 74(3): 103-18.
20) Crespo R, Ne E, Reinders J, et al. PCID2 dysregulates transcription and viral RNA processing to promote HIV-1 latency. iScience. 2024; 27(3): 109152.
21) Clarke BP, Gao S, Mei M, et al. Structural mechanism of DDX39B regulation by human TREX-2 and a related complex in mRNP remodeling. Nat Commun. 2025; 16(1): 5471.
22) Rezano A, Gondo N, Sakai Y, et al. Tumorigenesis caused by aberrant expression of GANP, a central component in the mammalian TREX-2 complex-lessons from transcription-coupled DNA damages. Int J Mol Sci. 2024; 25(24): 13612.
23) Li J, Zou C, Bai Y, et al. DSS1 is required for the stability of BRCA2. Oncogene. 2006; 25(8): 1186-94.
24) Zhao W, Vaithiyalingam S, San Filippo J, et al. Promotion of BRCA2-Dependent Homologous Recombination by DSS1 via RPA Targeting and DNA Mimicry. Mol Cell. 2015; 59(2): 176-87.
25) Huang Y, Li W, Foo T, et al. DSS1 restrains BRCA2's engagement with dsDNA for homologous recombination, replication fork protection, and R-loop homeostasis. Nat Commun. 2024; 15(1): 7081.
26) Faza MB, Kemmler S, Jimeno S, et al. Sem1 is a functional component of the nuclear pore complex-associated messenger RNA export machinery. J Cell Biol 2009; 184(6): 833-46.
27) Rezano A, Kuwahara K, Yamamoto-Ibusuki M, et al. Breast cancers with high DSS1 expression that potentially maintains BRCA2 stability have poor prognosis in the relapse-free survival. BMC Cancer. 2013; 13: 562.
28) Gondo N, Sakai Y, Zhang Z, et al. Increased chemosensitivity via BRCA2-independent DNA damage in DSS1- and PCID2-depleted breast carcinomas. Lab Invest. 2021; 101(8): 1048-59.
29) Chen X, Liu Q, Wu J, et al. DSS1 inhibits autophagy to acti-

vate epithelial-mesenchymal transition in a pro-metastatic niche of renal cell carcinoma. Nat Commun. 2025; 16(1): 6769.

30) Funakoshi M, Li X, Velichutina I, et al. Sem1, the yeast ortholog of a human BRCA2-binding protein, is a component of the proteasome regulatory particle that enhances proteasome stability. J Cell Sci. 2004; 117(Pt 26): 6447-54.

31) Schenstrøm SM, Rebula CA, Tatham MH, et al. Expanded Interactome of the Intrinsically Disordered Protein Dss1. Cell Rep. 2018; 25(4): 862-70.

32) Ruidiaz SF, Dreier JE, Hartmann-Petersen R, et al. The disordered PCI-binding human proteins CSNAP and DSS1 have diverged in structure and function. Protein Sci. 2021; 30(10): 2069-82.

33) Jacobsen NL, Bloch M, Millard PS, et al. Phosphorylation of Schizosaccharomyces pombe Dss1 mediates direct binding to the ubiquitin-ligase Dma1 in vitro. Protein Sci. 2023; 32(9): e4733.

34) Stefanovie B, Hengel SR, Mlcouskova J, et al. DSS1 interacts with and stimulates RAD52 to promote the repair of DSBs. Nucleic Acids Res. 2020; 48(2): 694-708.

35) Kuang Z, Ke J, Hong J, et al. Structural assembly of the nucleic-acid-binding Thp3-Csn12-Sem1 complex functioning in mRNA splicing. Nucleic Acids Res 2022; 50(15): 8882-97.

36) Fischer T, Strässer K, Rácz A, et al. The mRNA export machinery requires the novel Sac3p-Thp1p complex to dock at the nucleoplasmic entrance of the nuclear pores. EMBO J. 2002; 21(21): 5843-52.

37) Umlauf D, Bonnet J, Waharte F, et al. The human TREX-2 complex is stably associated with the nuclear pore basket. J Cell Sci. 2013; 126(Pt 12): 2656-67.

38) Schneider M, Hellerschmied D, Schubert T, et al. The nuclear pore-associated TREX-2 complex employs mediator to regulate gene expression. Cell. 2015; 162(5): 1016-28.

39) González-Aguilera C, Tous C, Gómez-González B, et al. The THP1-SAC3-SUS1-CDC31 complex works in transcription elongation-mRNA export preventing RNA-mediated genome instability. Mol Biol Cell. 2008; 19(10): 4310-8.

40) Strässer K, Bassler J, Hurt E. Binding of the Mex67p/Mtr2p heterodimer to FXFG, GLFG, and FG repeat nucleoporins is essential for nuclear mRNA export. J Cell Biol. 2000; 150(4): 695-706.

41) Herold A, Suyama M, Rodrigues JP, et al. TAP (NXF1) belongs to a multigene family of putative RNA export factors with a conserved modular architecture. Mol Cell Biol. 2000; 20(23): 8996-9008.

42) Braun IC, Herold A, Rode M, et al. Nuclear export of mRNA by TAP/NXF1 requires two nucleoporin-binding sites but not p15. Mol Cell Biol. 2002; 22(15): 5405-18.

43) Ginno PA, Lott PL, Christensen HC, et al. R-loop formation is a distinctive characteristic of unmethylated human CpG island promoters. Mol Cell. 2012; 45(6): 814-25.

44) Chen PB, Chen HV, Acharya D, et al. R loops regulate promoter-proximal chromatin architecture and cellular differentiation. Nat Struct Mol Biol. 2015; 22(12): 999-1007.

45) Sanz LA, Hartono SR, Lim YW, et al. Prevalent, dynamic, and conserved R-loop structures associate with specific epigenomic signatures in mammals. Mol Cell. 2016; 63(1): 167-78.

46) Skourti-Stathaki K, Kamieniarz-Gdula K, Proudfoot NJ. R-loops induce repressive chromatin marks over mammalian gene terminators. Nature. 2014; 516(7531): 436-9.

47) Skourti-Stathaki K, Proudfoot NJ, Gromak N. Human senataxin resolves RNA/DNA hybrids formed at transcriptional pause sites to promote Xrn2-dependent termination. Mol Cell. 2011; 42(6): 794-805.

48) Yu K, Chedin F, Hsieh CL, et al. R-loops at immunoglobulin class switch regions in the chromosomes of stimulated B cells. Nat Immunol. 2003; 4(5): 442-51.

49) Ramiro AR, Stavropoulos P, Jankovic M, et al. Transcription enhances AID-mediated cytidine deamination by exposing single-stranded DNA on the nontemplate strand. Nat Immunol. 2003; 4(5): 452-6.

50) Chaudhuri J, Tian M, Khuong C, et al. Transcription-targeted DNA deamination by the AID antibody diversification enzyme. Nature 2003; 422(6933): 726-30.

51) Muramatsu M, Kinoshita K, Fagarasan S, et al. Class switch recombination and hypermutation require activation-induced cytidine deaminase (AID), a potential RNA editing enzyme. Cell. 2000; 102(5): 553-63.

52) Xu B, Clayton DA. A persistent RNA-DNA hybrid is formed during transcription at a phylogenetically conserved mitochondrial DNA sequence. Mol Cell Biol 1995; 15(1): 580-9.

53) Xu B, Clayton DA. RNA-DNA hybrid formation at the human mitochondrial heavy-strand origin ceases at replication start sites: an implication for RNA-DNA hybrids serving as primers. EMBO J. 1996; 15(12): 3135-43.

54) Lee DY, Clayton DA. Properties of a primer RNA-DNA hybrid at the mouse mitochondrial DNA leading-strand origin of replication. J Biol Chem 1996; 271(39): 24262-9.

55) Lee DY, Clayton DA. Initiation of mitochondrial DNA replication by transcription and R-loop processing. J Biol Chem. 1998; 273(46): 30614-21.

56) Hamperl S, Bocek MJ, Saldivar JC, et al. Transcription-replication conflict orientation modulates R-loop levels and activates distinct DNA damage responses. Cell. 2017; 170(4): 774-86.e19.

57) Stoy H, Zwicky K, Kuster D, et al. Direct visualization of transcription-replication conflicts reveals post-replicative DNA:RNA hybrids. Nat Struct Mol Biol 2023; 30(3): 348-

59.
58) Promonet A, Padioleau I, Liu Y, et al. Topoisomerase 1 prevents replication stress at R-loop-enriched transcription termination sites. Nat Commun 2020; 11 (1) : 3940.
59) Hamperl S, Cimprich KA. The contribution of co-transcriptional RNA:DNA hybrid structures to DNA damage and genome instability. DNA Repair (Amst) . 2014; 19: 84-94.
60) Crossley MP, Bocek M, Cimprich KA. R-loops as cellular regulators and genomic threats. Mol Cell. 2019; 73 (3) : 398-411.
61) García-Muse T, Aguilera A. R loops: from physiological to pathological roles. Cell. 2019; 179 (3) : 604-18.
62) Allison DF, Wang GG. R-loops: formation, function, and relevance to cell stress. Cell Stress. 2019; 3 (2) : 38-46.
63) Sollier J, Cimprich KA. Breaking bad: R-loops and genome integrity. Trends Cell Biol. 2015; 25 (9) : 514-22.
64) Sollier J, Stork CT, García-Rubio ML, et al. Transcription-coupled nucleotide excision repair factors promote R-loop-induced genome instability. Mol Cell. 2014; 56 (6) : 777-85.
65) Li F, Zafar A, Luo L, et al. R-loops in genome instability and cancer. Cancers (Basel) . 2023; 15 (20) : 4986.
66) Dieppois G, Iglesias N, Stutz F. Cotranscriptional recruitment to the mRNA export receptor Mex67p contributes to nuclear pore anchoring of activated genes. Mol Cell Biol. 2006; 26 (21) : 7858-70.
67) Wickramasinghe VO, McMurtrie PI, Mills AD, et al. mRNA export from mammalian cell nuclei is dependent on GANP. Curr Biol. 2010; 20 (1) : 25-31.
68) Wickramasinghe VO, Andrews R, Ellis P, et al. Selective nuclear export of specific classes of mRNA from mammalian nuclei is promoted by GANP. Nucleic Acids Res. 2014; 42 (8) : 5059-71.
69) Tian L, Liu L, Yoon Y, et al. LENG8 mediates RNA nuclear retention and degradation in eukaryotes. Mol Cell. 2026; 86 (8) : 1478-94.e8.
70) Jensen RB, Carreira A, Kowalczykowski SC. Purified human BRCA2 stimulates RAD51-mediated recombination. Nature. 2010; 467 (7316) : 678-83.
71) Carreira A, Hilario J, Amitani I, et al. The BRC repeats of BRCA2 modulate the DNA-binding selectivity of RAD51. Cell. 2009; 136 (6) : 1032-43.
72) Schlacher K, Christ N, Siaud N, et al. Double-strand break repair-independent role for BRCA2 in blocking stalled replication fork degradation by MRE11. Cell. 2011; 145 (4) : 529-42.
73) Yang H, Jeffrey PD, Miller J, et al. BRCA2 function in DNA binding and recombination from a BRCA2-DSS1-ssDNA structure. Science. 2002; 297 (5588) : 1837-48.
74) Kristensen CN, Bystol KM, Li B, et al. Depletion of DSS1 protein disables homologous recombinational repair in human cells. Mutat Res. 2010; 694 (1-2) : 60-4.
75) Lee M, Shorthouse D, Mahen R, et al. Cancer-causing BRCA2 missense mutations disrupt an intracellular protein assembly mechanism to disable genome maintenance. Nucleic Acids Res. 2021; 49 (10) : 5588-604.
76) Gudmundsdottir K, Lord CJ, Witt E, et al. DSS1 is required for RAD51 focus formation and genomic stability in mammalian cells. EMBO Rep. 2004; 5 (10) : 989-93.
77) Le HP, Ma X, Vaquero J, et al. DSS1 and ssDNA regulate oligomerization of BRCA2. Nucleic Acids Res. 2020; 48 (14) : 7818-33.
78) Shivji MKK, Renaudin X, Williams ÇH, et al. BRCA2 regulates transcription elongation by RNA polymerase II to prevent R-loop accumulation. Cell Rep. 2018; 22 (4) : 1031-9.
79) Sessa G, Gómez-González B, Silva S, et al. BRCA2 promotes DNA-RNA hybrid resolution by DDX5 helicase at DNA breaks to facilitate their repair. EMBO J. 2021; 40 (7) : e106018.
80) D'Alessandro G, Whelan DR, Howard SM, et al. BRCA2 controls DNA:RNA hybrid level at DSBs by mediating RNase H2 recruitment. Nat Commun. 2018; 9 (1) : 5376.
81) Bhatia V, Barroso SI, García-Rubio ML, et al. BRCA2 prevents R-loop accumulation and associates with TREX-2 mRNA export factor PCID2. Nature. 2014; 511 (7509) : 362-5.
82) González-Martín A, Pothuri B, Vergote I, et al. Niraparib in Patients with Newly Diagnosed Advanced Ovarian Cancer. N Engl J Med. 2019; 381 (25) : 2391-402.
83) Agarwal N, Azad AA, Carles J, et al. Talazoparib plus enzalutamide in men with metastatic castration-resistant prostate cancer: final overall survival results from the randomised, placebo-controlled, phase 3 TALAPRO-2 trial. Lancet. 2025; 406 (10502) : 447-60.

Case Report

Faggot cells in acute myeloid leukemia with *NUP98*::*HOXA9*

Makyo Ueda[*1], Saori Oishi*[*1], Norihiko Amemiya*[*1], Daisuke Osada*[*1],
Megumi Yamada*[*2], Fuminori Kazama*[*1], Ayato Nakadate*[*2], Ichiro Kawashima*[*2],
Keita Kirito*[*2], †Katsue Suzuki-Inoue*[*1,3]

†Correspondence: Department of Clinical and Laboratory Medicine, Faculty of Medicine, University of Yamanashi, 1110 Shimokato, Chuo, Yamanashi 409-3898, Japan. E-mail: katsuei@yamanashi.ac.jp
Received January 27, 2026; accepted March 13, 2026
*[1] Department of Clinical Laboratory, University of Yamanashi Hospital, Yamanashi, Japan
*[2] Department of Hematology and Oncology, University of Yamanashi, Yamanashi, Japan
*[3] Department of Clinical and Laboratory Medicine, Faculty of Medicine, University of Yamanashi, Yamanashi, Japan

ABSTRACT

Faggot cells are abnormal cells containing multiple Auer rods in the cytoplasm. They are usually found in acute promyelocytic leukemia (APL), typically characterized by *PML*::*RARA* fusion. We describe a rare case in which faggot cells were observed, but the patient was ultimately diagnosed with acute myeloid leukemia (AML) with *NUP98*::*HOXA9*. A man in his 40s presented with fever, pneumonia, and coagulopathy. Peripheral blood examination revealed an increased number of blast cells with Auer rods. Bone marrow (BM) aspirate smears showed the proliferation of abnormal promyelocyte-like cells showing strong myeloperoxidase positivity; some contained multiple Auer rods, consistent with faggot cells. Flow cytometric analysis of the BM revealed an APL-like immunophenotype, characterized by the expression of myeloid markers and the absence of CD34 and HLA-DR. Based on these morphological and immunophenotypic findings, the patient was initially suspected to have APL and was treated with all-trans retinoic acid (ATRA) in combination with cytotoxic induction chemotherapy. However, subsequent molecular analyses revealed the presence of *NUP98*::*HOXA9* mRNA and absence of *PML*::*RARA* mRNA. Therefore, APL was excluded, and the patient was diagnosed with AML with *NUP98* rearrangement. Consequently, ATRA was discontinued. Chromosomal analysis revealed the presence of t(7;11)(p15;p15), supporting the revised diagnosis. Despite exhibiting APL-like morphological and immunophenotypic features, the disease was ultimately diagnosed as non-APL AML based on genetic and chromosomal testing. This case highlights the fact that faggot cells are not entirely specific for APL and emphasizes the importance of integrating morphological, immunophenotypic, and genetic/cytogenetic findings for accurate diagnosis and appropriate treatment.

〔Lab Med Int 2026; 5(2): 78-83〕

Key Words
faggot cells, Auer rods, acute myeloid leukemia, *NUP98*::*HOXA9*

I. Introduction

In hematological malignancies such as acute myeloid leukemia (AML), it is necessary to combine morphological examination, flow cytometry, chromosomal analysis, and genetic testing to make an accurate diagnosis and enable appropriate treatment planning. Although a traditional method, morphological examination contributes to clinical practice as a method with the advantage of rapid performance, often aiding clinical decision-making in specific contexts.

Faggot cells are abnormal myeloid cells that contain multiple Auer rods within their cytoplasm. These cells are considered characteristic findings of acute promyelocytic leukemia (APL), which is typically caused by the *PML*::*RARA* fusion gene. Here, we report a case in

which faggot cells were morphologically observed; however, chromosomal and genetic findings ultimately led to the diagnosis of non-APL AML, specifically AML with *NUP98*::*HOXA9* fusion.

II. Case report

A man in his 40s visited his previous physician because of a fever. Radiological examination revealed an infiltrative shadow in the upper left lobe of the lung. Blood tests revealed severe inflammation, thrombocytopenia, and elevated levels of fibrin/fibrinogen degradation products (FDP). Consequently, the patient was admitted with diagnoses of pneumonia and coagulopathy. A subsequent peripheral blood (PB) smear revealed an increased number of blast cells with Auer rods, leading to a referral and transfer to our hospital with suspected AML.

Blood tests conducted at our hospital yielded the following results: white blood cell count, 13.58 × 10^9/L (blast cells: 84.5%, neutrophils: 8.0%, and lymphocytes: 7.5%); red blood cell count, 2.63 × 10^{12}/L; hemoglobin, 9.3 g/dL; platelet count, 54 × 10^9/L; lactate dehydrogenase, 619 U/L; prothrombin time, 13.2 s; activated partial thromboplastin time, 22.1 s; fibrinogen, 455 mg/dL; FDP, 33.3 μg/mL; thrombin-antithrombin complex, 4.9 ng/mL; and plasmin-alpha2-plasmin inhibitor-complex, 6.8 μg/mL. In the PB smear, the cells counted as blast cells were large with a fine chromatin network, clear nucleoli, and cytoplasm containing fine granules. Some contained a single Auer rod (**Figure 1A**). A bone marrow (BM) aspirate smear showed hypercellular marrow with proliferation of abnormal promyelocyte-like cells. These cells were medium-to-large, with a basophilic cytoplasm, often containing fine granules. They exhibited a nuclear-to-cytoplasmic ratio of ≥ 50%, a fine chromatin network, and distinct nucleoli. Some cells contained one or more Auer rods, resembling the faggot cells observed in patients with APL (**Figure 1B–D**). Based on these morphological features, these cells were counted as promyelocytes, resulting in 57.6% promyelocytes. In addition, 13.8% of the cells were blast cells, similar to those observed in the PB smears. Promyelocytes were strongly positive for myeloperoxidase (MPO) staining. Pseudo–Pelger–Huët neutrophils were also observed, although only as a subtle and minor finding. BM flow cytometry analysis showed that the CD45-dim cell population was positive for CD13 (65.6%) and CD33 (98.4%) and negative for CD3, CD19,

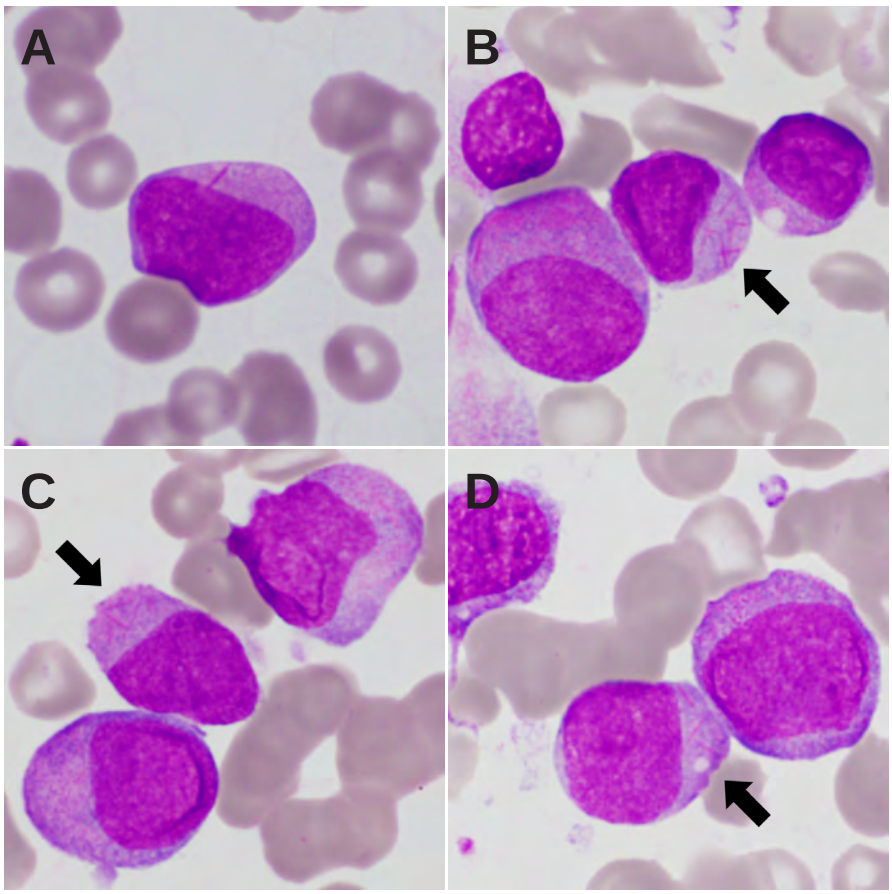

Figure 1 May-Grünwald-Giemsa stain; magnification, 1000 ×. (**A**) Peripheral blood smear showing the blast cell with a single Auer rod. (**B-D**) Bone marrow aspirate smear showing faggot cells (arrows).

CD34, CD41, and HLA-DR (**Figure 2**). Based on the morphological features and flow cytometry findings, the patient was initially suspected to have APL and was treated with all-trans retinoic acid (ATRA) in combination with cytotoxic induction chemotherapy.

On day 4 after initiating the induction therapy, results of the real-time polymerase chain reaction screening for leukemia chimeric genes in the BM became available. The screening revealed the presence of *NUP98*::*HOXA9* mRNA (2.7×10^4 copies/μg RNA) and absence of *PML*::*RARA* mRNA. Based on these findings, APL was ruled out, and the patient was diagnosed with AML with *NUP98* rearrangement. Accordingly, ATRA was discontinued. Subsequent chromosomal analysis using G-banding confirmed a karyotype of 46,XY,t(7;11)(p15;p15)[15]/46,XY[5], corresponding to the exclusion of APL and presence of *NUP98*::*HOXA9* fusion (**Figure 3**). Other genetic testing was negative for *FLT3*-internal tandem duplication. Cytotoxic induction therapy was continued, and a complete hematological remission was confirmed on day 29 by BM examination. After completing three courses of consolidation chemotherapy, the patient underwent allogeneic BM transplantation during the first complete remission. However, approximately 9 months later, the AML relapsed. In the PB and BM aspirate smears, blast cells increased, but no faggot cells were observed. The reinduction chemotherapy led to a reduction in blast cells, and umbilical cord blood transplantation was planned. However, the patient died due to the exacerbation of organizing pneumonia.

III. Discussion

Faggot cells are mostly observed in APL. Although their presence has also been reported in non-APL settings such as AML with inv(16) or myelodysplastic neoplasms, they are extremely rare[1)-3)]. In this non-APL AML case, we discuss the possible mechanisms underlying the appearance of faggot cells and describe the associated morphological characteristics.

Azurophilic granules are cytoplasmic particles that are stained purple-brown to purple-red with azure dyes. In granulocytes, these granules correspond to primary granules and contain antimicrobial substances such as MPO. During granulocyte differentiation, primary gran-

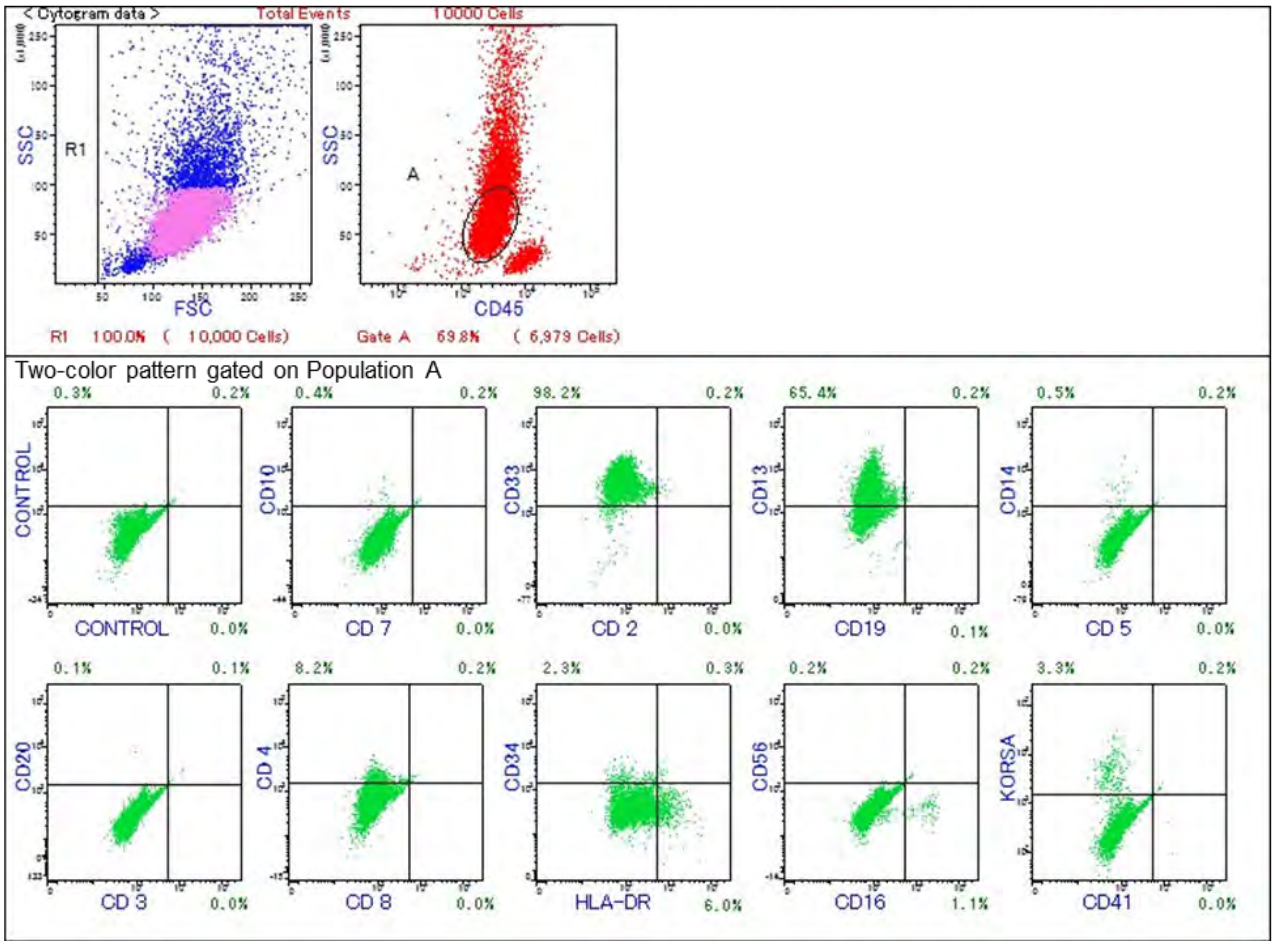

Figure 2 Flow cytometric analysis of cell surface markers in bone marrow aspirate: Two-color pattern gated on Population A.

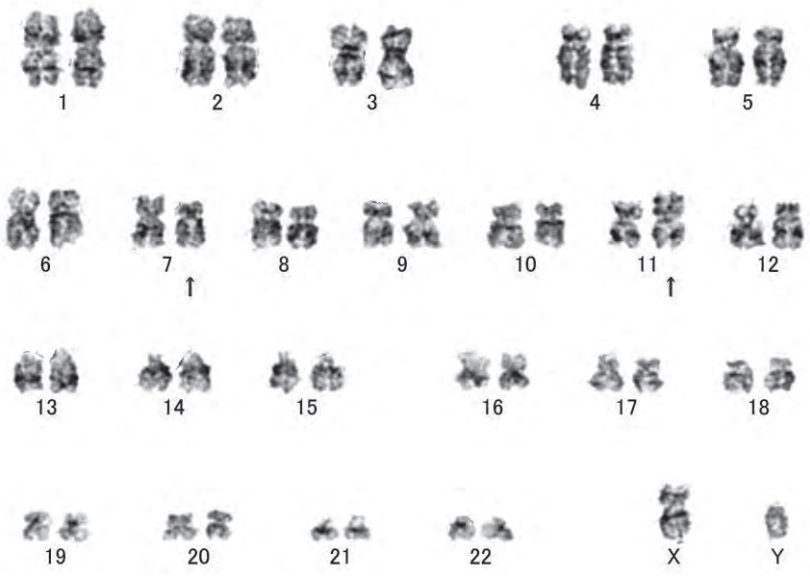

Figure 3 Chromosomal analysis using G-banding, showing translocation t(7;11)(p15;p15) in 15 of the 20 analyzed cells.

ule production ceases at the myelocyte stage, after which specific granules, called secondary granules, begin to form. Auer rods are reddish-purple, needle- or rod-shaped cytoplasmic inclusions thought to be azurophilic granules that fail to mature normally and fused together[4]. They are found in leukemic cells, but not in normal cells, and their presence in acute leukemia strongly suggests AML. Auer rods are typically observed in myeloblasts and promyelocytes and may appear singly or in multiples within the cytoplasm. Cells containing bundles of Auer rods are termed faggot cells and are characteristically found in the abnormal promyelocytes of APL[5].

AML with *NUP98*::*HOXA9* fusion is rare, has a poor prognosis, and is caused by a translocation t(7;11)(p15;p15). NUP98 is one of the proteins that constitute the nuclear pore complex and is involved in the transport of mRNA and proteins between the nucleus and cytoplasm[6]. *HOXA* is one of the clusters of *HOX* genes that encode transcription factors with a DNA-binding domain[6]. The expression level of *HOXA9* is normally downregulated during hematopoietic differentiation. However, in this disease, continuous activation of *HOXA9* by the NUP98 promoter due to the *NUP98*::*HOXA9* fusion is thought to inhibit normal hematopoietic differentiation[6)-9)].

The *PML*::*RARA* fusion, typically responsible for APL, represses RARα-dependent transcription, thereby blocking myeloid differentiation at the promyelocyte stage[10]. Accordingly, typical APL exhibits an immunophenotype of $CD13^+$, $CD33^+$, $CD34^-$, and $HLA\text{-}DR^-$. This pattern, characterized by positivity for myeloid lineage markers (CD13 and CD33), coupled with the loss of early precursor markers (CD34 and HLA-DR), indicates that the cells have progressed to the promyelocyte-like stage. Notably, the immunophenotype at the initial onset in the present case was similar, suggesting arrest at a similar promyelocyte-like stage. Therefore, we hypothesized that the arrest of leukemic cell differentiation at this promyelocyte-like stage may have contributed to the accumulation of Auer rods, resulting in the formation of faggot cells. Conversely, the immunophenotypes of the CD45-dim population at the time of recurrence were $CD13^+$, $CD33^+$, $CD34^+$, and $HLA\text{-}DR^{weakly+}$, indicating the proliferation of more immature cells relative to the initial onset; no faggot cells were observed. Most AML cases with *NUP98*::*HOXA9* fusion are classified as AML M2 according to the French-American-British (FAB) classification[11),12)]. Nevertheless, unlike typical cases, leukemic cells at the initial onset in the present case appeared to show differentiation arrest, particularly at the promyelocyte-like stage; the precise mechanism underlying this remains unclear.

Morphologically, the Auer rod bundles in this case appeared thinner and longer than those typically observed in APL. Additionally, pseudo–Pelger–Huët anomaly, which is usually absent in APL, was identified in some neutrophils. These findings resemble the characteristic features of AML with *RUNX1*::*RUNX1T1* fusion[4),13)]. To our knowledge, only two cases of faggot cells being found in AML with *NUP98*::*HOXA9* fusion have been reported globally[14)-16)], and further accumulation of cases is essential to clarify these morphological features from those of APL.

The need for an integrated diagnostic approach was

evident in this case. Accurate diagnosis is of paramount importance because hematopoietic tumors encompass various subtypes, each requiring distinct treatment approaches and presenting with different prognoses. As evidenced by the continued use of the FAB classification proposed in 1976, the careful observation of blood cells is essential[11]. APL is a prime example of a condition in which rapid diagnosis is critical, and morphology contributes significantly. APL frequently presents with a high complication rate of disseminated intravascular coagulation accompanied by life-threatening hyperfibrinolysis, making early diagnosis and immediate treatment crucial. Therefore, when faggot cells are observed, it is prudent to suspect APL and initiate ATRA therapy[2]. However, if the disease is not APL, the treatment approach may be ineffective and unnecessary. Thus, methods other than morphological testing, specifically genetic and chromosomal testing, are essential for a definitive diagnosis of APL. In the present case, although the disease displayed APL-like morphological characteristics and immunophenotypes, genetic and chromosomal testing ultimately ruled out APL. Collectively, an integrated diagnostic approach utilizing complementary techniques is essential for an accurate diagnosis and appropriate treatment; findings from the present case reinforce this necessity.

Authorship contributions

MU drafted the manuscript. MU, SO, NA, and DO performed morphological examinations. MU and NA captured microscopic images. MY, AN, IK, and KK were physicians involved in patient care. SO, FK, and KS-I revised the manuscript. All the authors have read and approved the final version of the manuscript.

Disclosure of conflicts of interest

The authors declare no conflicts of interest associated with this manuscript.

Funding

None.

Acknowledgements

We would like to thank Editage (www.editage.jp) for English language editing.

Previous abstract presentation

The abstract of this report was presented at the 26th Annual Meeting of the Japanese Society for Laboratory Hematology (Kyoto International Conference Center, Kyoto, 2025).

References

1) Garrastazul-Sánchez MP, Vilches-Moreno M, Fernández-Valle MC, et al. Neutrophil faggot cells and inv(16): Not such a fortuitous association? Ann Hematol. 2019; 98 (5): 1293-5. doi: 10.1007/s00277-018-3484-5.

2) Kim JA, Shin WY, Kim J, et al. A case of acute myeloid leukemia with inv(16)(p13.1q22);*CBFB-MYH11* presenting with faggot cells. Ann Lab Med. 2021; 41(3): 333-5. doi: 10.3343/alm.2021.41.3.333.

3) Ogura H, Inagaki A, Wakita A. A case of myelodysplastic syndrome presenting with faggot-like cells. Int J Hematol. 2013; 97 (4): 443-5. doi: 10.1007/s12185-013-1306-z.

4) Sehgal T, Sharma P. Auer rods and faggot cells: A review of the history, significance and mimics of two morphological curiosities of enduring relevance. Eur J Haematol. 2023; 110 (1): 14-23. doi: 10.1111/ejh.13872.

5) Jerez A, del Mar Osma M, Amigo M, et al. Faggot cells in an HIV-positive patient with inv(16)/therapy-related acute myeloid leukaemia. Br J Haematol. 2010; 150(6): 646. doi: 10.1111/j.1365-2141.2010.08294.x.

6) Gough SM, Slape CI, Aplan PD. NUP98 gene fusions and hematopoietic malignancies: Common themes and new biologic insights. Blood. 2011; 118 (24): 6247-57. doi: 10.1182/blood-2011-07-328880.

7) Borrow J, Shearman AM, Stanton VP Jr, et al. The t(7;11) (p15;p15) translocation in acute myeloid leukaemia fuses the genes for nucleoporin *NUP98* and class I homeoprotein *HOXA9*. Nat Genet. 1996; 12 (2): 159-67. doi: 10.1038/ng0296-159.

8) Takeda A, Goolsby C, Yaseen NR. NUP98-HOXA9 induces long-term proliferation and blocks differentiation of primary human $CD34^+$ hematopoietic cells. Cancer Res. 2006; 66 (13): 6628-37. doi: 10.1158/0008-5472.CAN-06-0458.

9) Nakamura T, Largaespada DA, Shaughnessy JD Jr, et al. Cooperative activation of *Hoxa* and *Pbx1*-related genes in murine myeloid leukaemias. Nat Genet. 1996; 12 (2): 149-53. doi: 10.1038/ng0296-149.

10) Dos Santos GA, Kats L, Pandolfi PP. Synergy against PML-RARa: targeting transcription, proteolysis, differentiation, and self-renewal in acute promyelocytic leukemia. J Exp Med. 2013; 210 (13): 2793-802. doi: 10.1084/jem.20131121.

11) Bennett JM, Catovsky D, Daniel MT, et al. Proposals for the classification of the acute leukaemias. French-American-British (FAB) co-operative group. Br J Haematol. 1976; 33 (4): 451-8. doi: 10.1111/j.1365-2141.1976.tb03563.x.

12) Huang SY, Tang JL, Liang YJ, et al. Clinical, haematological and molecular studies in patients with chromosome translocation t(7;11): A study of four Chinese patients in Taiwan. Br J Haematol. 1997; 96(4): 682-7. doi: 10.1046/j.1365-2141.1997.d01-2100.x

13) Nakamura H, Kuriyama K, Sadamori N, et al. Morphological subtyping of acute myeloid leukemia with maturation (AML-M2): Homogeneous pink-colored cytoplasm of mature neutrophils is most characteristic of AML-M2 with t(8;21). Leukemia. 1997; 11 (5): 651-5. doi: 10.1038/sj.leu.2400618.

14) Yanagisawa H, Mizuta S, Kawabata H, et al. Faggot cells in acute myeloid leukemia with t(7;11)(p15;p15) and *NUP98-HOXA9* fusion. Ann Hematol. 2021; 100 (8): 2121-3. doi: 10.1007/s00277-020-04122-2.

15) Lin E, Chen W. Acute myeloid leukemia with *NUP98*::*HOXA9* mimicking acute promyelocytic leukemia. Blood. 2023; 142 (21): 1845. doi: 10.1182/blood.2023022102.

16) Sajjan S, Oertling E, Fuda F, et al. Clinicopathologic and molecular characterization of *NUP98*-rearranged acute leukemias. Int J Lab Hematol. 2025; 47 (3): 445-53. doi: 10.1111/ijlh.14422.